ONSET OF DECONFINEMENT IN NUCLEUS–NUCLEUS COLLISIONS: REVIEW FOR PEDESTRIANS AND EXPERTS

Marek Gazdzicki[a,b], Mark Gorenstein[c,d], Peter Seyboth[e,b]

[a]Institut für Kernphysik, University of Frankfurt, Frankfurt, Germany
[b]Jan Kochanowski University, Kielce, Poland
[c]Bogolyubov Institute for Theoretical Physics, Kiev, Ukraine
[d]Frankfurt Institute for Advanced Studies, Frankfurt, Germany
[e]Max-Planck-Institut fuer Physik, Munich, Germany

(Received January 31, 2011; revised version received February 7, 2011)

Evidence for the energy threshold of creating the quark-gluon plasma in nucleus–nucleus collisions, the so-called onset of deconfinement, has been found by the energy scan program of the NA49 experiment at the CERN SPS. In this paper we review the experimental and theoretical status of this phenomenon. First, the basic, qualitative ideas are presented for non-experts. Next, the latest experimental results are compared to a statistical model within which the onset of deconfinement and its signals had been predicted. Finally, alternative interpretations and open questions are discussed.

DOI:10.5506/APhysPolB.42.307
PACS numbers: 25.75.Nq, 25.75.Dw, 25.75.Ag, 24.10.Pa

1. Introduction

One of the important issues of contemporary physics is the understanding of strong interactions and in particular the study of the properties of strongly interacting matter in equilibrium. What are the phases of this matter and what do the transitions between them look like? These questions motivate broad experimental and theoretical efforts since more than 40 years. The study of high energy collisions between two atomic nuclei give us the unique possibility to address these issues in well controlled laboratory experiments. In particular, the advent of the quark model of hadrons and the development of the commonly accepted theory of strong interactions, quantum chromodynamics (QCD), naturally led to expectations that matter at very high densities may exist in a state of quasi-free quarks and gluons, the quark-gluon plasma (QGP) [1, 2, 3].

Experimental searches for QGP signals started at the Super Proton Synchrotron (SPS) of the European Organization for Nuclear Research (CERN) and the Alternating Gradient Synchrotron (AGS) of Brookhaven National Laboratory (BNL) in the mid 1980s. Today they are pursued also at much higher collision energies at the Relativistic Heavy Ion Collider (RHIC) at BNL. Soon experiments on nucleus–nucleus collisions at the Large Hadron Collider (LHC) in CERN will join the world effort at energies 20 times higher than at RHIC. Most probably that the QGP is formed at the early stage of heavy ion collisions at the top SPS energy and at RHIC energies. Unambiguous evidence of the QGP state was, however, missing. This may be attributed to the difficulty of obtaining unique and quantitative predictions of the expected QGP signals from the theory of strong interactions.

For this reason the NA49 Collaboration at the CERN SPS has searched over the past years for signs of the onset of QGP creation in the energy dependence of hadron production properties. This search was motivated by a statistical model [4] showing that the onset of deconfinement should lead to rapid changes of the energy dependence of numerous experimentally detectable properties of the collisions, all appearing in a common energy domain. The predicted features have recently been observed [5] and dedicated experiments now continue detailed studies in the energy region of the onset of deconfinement.

It is thus time for a summary. In this paper we review the experimental and theoretical status of the onset of deconfinement. First, the basic qualitative ideas are presented for non-experts. Next, a quantitative model within which the onset of deconfinement and its signals were predicted is reexamined and compared with the latest experimental results. Finally, alternative interpretations and open questions are discussed.

2. Onset of deconfinement for pedestrians

Phase transitions are fascinating physical phenomena. Small changes in temperature or pressure lead to dramatic changes in macroscopic properties of matter. Common examples from our daily life are transitions between solids, liquids and gases like boiling and freezing of water. The well known phase diagram of water is shown in Fig. 1, where the regions of existence of the various phases of water are depicted in a diagram of pressure and temperature. When adding heat to water one increases its temperature moving through its different phases and crossing their boundaries, as indicated by the dashed arrow in Fig. 1 for the example of constant atmospheric pressure. Dependence of the water temperature on the amount of added heat, called the heating curve of water, is shown in Fig. 2. In pure phases, such as ice, water or vapor, the temperature increases monotonically with added heat.

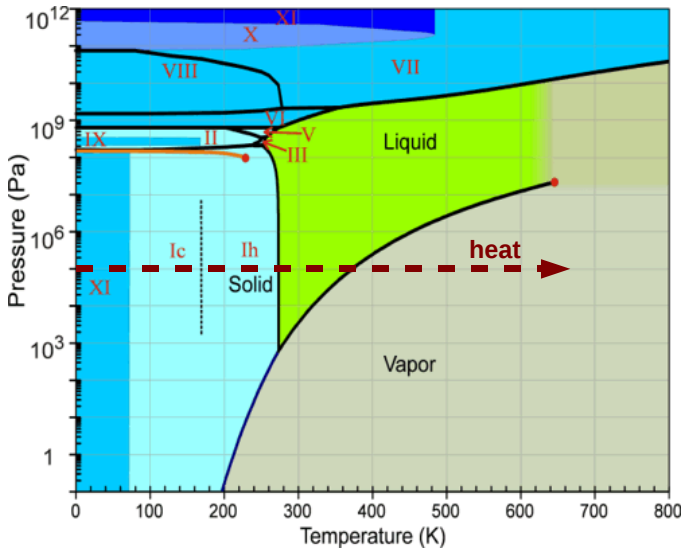

Fig. 1. Phases of water. When adding heat (energy) at constant pressure water is transformed from solid to liquid and then from liquid to vapor as indicated by the dashed arrow.

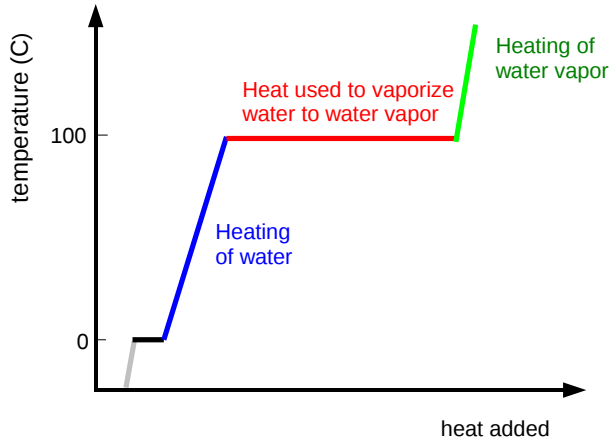

Fig. 2. Heating curve of water at fixed atmospheric pressure. It corresponds to the trajectory in the phase diagram of water indicated by the dashed arrow in Fig. 1.

The two regions of constant temperature (steps) signal the ice–water and water–vapor phase transitions. In these mixed phase regions added heat is used for the phase transformation instead of the increase of temperature as in the pure phase regions.

Properties of water and other substances surrounding us and the transitions between their various phases are determined by electromagnetic interactions of atoms and molecules. On the other hand, the properties of atomic nuclei which are built from nucleons (protons and neutrons) are determined by strong interactions. Naturally, the question arises whether strongly interacting matter also exists in distinct phases. What are their properties? At which temperatures do the transitions between them take place? What do these transitions look like?

Since more than 40 years it is known that hadrons (*i.e.* mesons and baryons; all strongly interacting particles observed in nature are called hadrons) consist of more elementary particles, the quarks and gluons. However, isolated quarks or gluons were never observed. They seem to be always confined in the interior of hadrons. But could a different phase of strongly interacting matter exist in which quarks and gluons are deconfined?

There are 3 parameters which describe the thermodynamical properties of a system. In non-relativistic systems they are temperature, particle number density, and pressure. The equation of state connects them, *e.g.*, the pressure is a well defined function of temperature and particle density for a specific substance. In experiments on water one can most easily fix temperature and pressure to define the point on the phase diagram in Fig. 1. Unlike in water, the number of particles is not conserved in strongly interacting relativistic matter. Instead of particle number density the baryonic number, *i.e.* the difference between the number of baryons and anti-baryons, is conserved. In calculations it is convenient to use the equivalent variables baryonic number density or baryonic chemical potential. The phase diagram of strongly interacting matter emerging from theoretical considerations and experimental results is shown in Fig. 3 in terms of the commonly used variables temperature and baryonic chemical potential. Laboratory experiments (see discussion below) can create strongly interacting matter with different temperatures T and baryonic chemical potentials μ_B. The functional dependence of the pressure on T and μ_B, *i.e.* the equation of state of strongly interacting matter, remains the subject of intensive experimental and theoretical studies.

A transition between the deconfined and the confined phase of strongly interacting matter probably took place during the expansion and cooling of the early Universe, about 1 microsecond after the Big Bang. Cosmological signatures of this transition are difficult to identify today. However, extremely dense strongly interacting matter fills the interior of neutron stars. Arguments in favor of the existence of quark matter in the center of such stars were advanced already in the 1960s, soon after formulation of the quark hypothesis. One of the pioneering papers [2] argued: "A neutron has a radius of about 0.5–1 fm (1 fm = 10^{-15} m), and so has a density of about

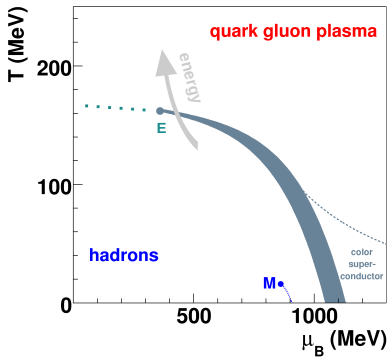

Fig. 3. Phases of strongly interacting matter. With increasing collision energy the matter created at the early stage of nucleus–nucleus collisions changes its properties as indicated by the arrow. At low energy it is in the confined phase (hadrons), at sufficiently high energy in the deconfined phase (QGP). M is the critical point of the nuclear liquid-gas phase transition. The shaded band shows the 1^{st} order phase boundary between the hadron and QGP phase which is expected to end in a critical end point E. At E the sharp phase transition turns into a rapid crossover indicated as the dotted line.

8×10^{14} g cm^{-3}, whereas the central density of a neutron star can be as much as 10^{16}–10^{17} g cm^{-3}. In this case, one must expect the hadrons to overlap, and their individuality to be confused. Therefore, we suggest that matter at such densities is a quark soup". The creation of matter in a deconfined phase, *i.e.* in the QGP phase, may be the only possibility to 'see' quarks and gluons moving freely in a large volume.

Cosmological and astrophysical objects with the required properties are, unfortunately, difficult to investigate. Systematic study of the properties of strongly interacting matter requires a method to create it under well controlled conditions in the laboratory. The study of collisions of two heavy nuclei gives us this possibility. Such a collision produces a droplet of strongly interacting matter of high energy density, the so-called fireball. It is natural to expect that with increasing collision energy the fireball energy density also increases. Thus, like in the case of water heating and observing successive transitions between its phases, we hope that with increasing collision energy we can detect anomalies in the energy dependence of hadron production properties and thus discover successive transitions between various phases of strongly interacting matter created at the early stage of collisions. The arrow in Fig. 3 schematically traces the position of the initially created fireball on the phase diagram when the energy of nucleus–nucleus collisions

is increasing. At sufficiently high collision energy this matter droplet may reach the QGP phase (see Fig. 3). Unfortunately the life time of the fireball is very short, about 10^{-22} seconds. It quickly expands, cools down (see Fig. 4) and finally decays into hadrons and a few light nuclei. These decay products are measured in detectors surrounding the collision point.

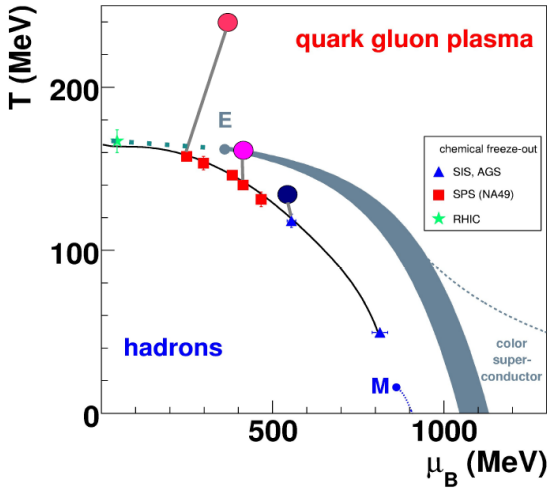

Fig. 4. Parameters of strongly interacting matter created at the early stage of nucleus–nucleus interactions are shown by the full circles for central Pb + Pb (Au + Au) collisions at the top AGS energy ($\sqrt{s_{NN}} \approx 5.5$ GeV), intermediate SPS energy ($\sqrt{s_{NN}} \approx 7.6$ GeV) and top SPS energy ($\sqrt{s_{NN}} \approx 17$ GeV). The created fireball expands and cools along trajectories indicated by solid lines and decouples at the freeze-out points (full squares, triangles and star).

The first phase transition of strongly interacting matter was observed studying collisions at very low energies [6] (the energy per nucleon–nucleon pair in the center of mass system $\sqrt{s_{NN}} < 2$ GeV). This transition between a nuclear liquid and a nuclear gas happens at a temperature of about 6×10^{10} K (5 MeV). The phase transition line and critical point M lie at large μ_B and small T inside the hadron phase region of the phase diagram as shown in Figs. 3 and 4.

Emerging results from the study of high energy collisions of nuclei confirm the existence of the second phase transition in strongly interacting matter which was suggested by QCD. It is the so-called deconfinement phase transition. Let us briefly present how one looked for this phase transition, and explain the main results.

The search for the phase of deconfined strongly interacting matter, the QGP, already has a long history. It received a boost from the first acceleration of oxygen and sulfur nuclei at the CERN SPS in 1986 ($\sqrt{s_{NN}} \approx 20$ GeV) and of lead nuclei in 1994 ($\sqrt{s_{NN}} \approx 17$ GeV). Measurements from an array of experiments indicated that the critical energy density was probably exceeded and matter with unusual properties appeared to be formed in the early stage of the collisions [7]. A key problem was the identification of experimental signatures of QGP creation. Several signatures of the formation of a transient QGP state during the early stage of the collision had been proposed in the past [8,9]. However, the uniqueness of these signatures came under renewed scrutiny and they were found not to be specific for the creation of QGP (see Appendix A for details).

In the mid 1990s a study of results from experiments at CERN and the AGS at BNL (maximum energy $\sqrt{s_{NN}} \approx 5.5$ GeV) raised [10,11] intriguing questions concerning the energy dependence of hadron production between top AGS and SPS energies. In response to these questions, a statistical model of the early stage of the collision process was proposed [4] in which an equation of state with a 1$^{\text{st}}$ order phase transition was assumed. In this model the onset of deconfinement led to the prediction of a non-monotonic collision energy dependence of several hadron production properties. In particular, the model predicted a sharp maximum in the ratio of multiplicities of strange hadrons (the hadrons which contain s and $\overline{s}$ quarks) to pions (the lightest hadron) at the beginning of the transition region, at about $\sqrt{s_{NN}} \approx 7.5$ GeV. This prediction triggered an extension of the experimental program at the SPS, the energy scan program [12]. Within this program head-on (central) collisions of two lead nuclei (Pb + Pb) were registered at several lower SPS energies ($\sqrt{s_{NN}} = 6.3$, 7.6, 8.7 and 12.3 GeV) by the NA49 experiment. Other heavy ion experiments at the SPS (NA45, NA50, NA57 and NA60) participated in selected runs of this program [13]. Final results, obtained mainly by the NA49 Collaboration, confirm the qualitative expectations and the quantitative predictions of the model: rapid changes in properties of hadron production occur within a narrow energy range, $\sqrt{s_{NN}} = 7$–12 GeV [5].

The most dramatic effect is seen in the energy dependence of the ratio of total particle yields of kaons and pions, $\langle K^+ \rangle / \langle \pi^+ \rangle$, in central Pb + Pb collisions which is plotted in Fig. 5, left. Following a fast threshold rise the ratio passes through a sharp maximum in the SPS range and then seems to settle to a plateau value at higher energies. Kaons are the lightest strange hadrons and due to approximate isospin symmetry the $\langle K^+ \rangle$ yield counts about half of the strange (anti-)quarks produced in the collisions and contained in the reaction products (see Appendix B for details). Thus Fig. 5, left demonstrates that the fraction of strangeness carrying particles in the

produced matter passes through a sharp maximum at the SPS in nucleus–nucleus collisions. This feature is not observed for proton–proton reactions as shown by the open dots in Fig. 5, left.

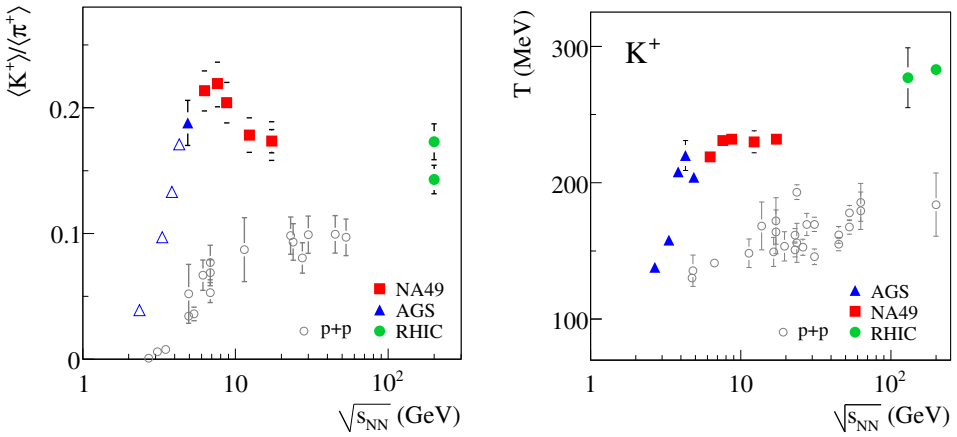

Fig. 5. Heating curves of strongly interacting matter. Hadron production properties (see text for details) are plotted as a function of collision energy for central Pb + Pb (Au + Au) collisions (upper set of points) and $p+p$ interactions (lower set of points) [5].

A second important result is the stationary value of the apparent temperature T of K^+ mesons in central Pb + Pb collisions at SPS energies as shown in Fig. 5, right. In the fireball picture the apparent temperature is related to the local random motion of the particles and their collective expansion velocity in the direction transverse to the collision axis.

Presently the sharp maximum and the following plateau in the energy dependence of the $\langle K^+\rangle/\langle\pi^+\rangle$ ratio has only been reproduced by the statistical model of the early stage. In this model it reflects the decrease in the ratio of strange to non-strange number of degrees of freedom when deconfinement sets in. The stationary value of the apparent temperature of K^+ mesons was predicted [14, 15, 16] as a consequence of the constant pressure and temperature at the early stage of nucleus–nucleus collisions in the SPS energy range due to the coexistence of hadronic and deconfined phases.

These results serve as evidence that the deconfinement phase transition in Pb + Pb collisions starts in the SPS energy range. The exciting and rich physics which can be studied in nucleus–nucleus collisions at the CERN SPS energies motivates ongoing and future experimental programs at the CERN SPS [17, 18], BNL RHIC [19], FAIR SIS [20] and JINR NICA [21].

3. Statistical Model of the Early Stage (SMES)

The experimental search for the onset of deconfinement performed by the experiment NA49 at the CERN SPS was motivated by the predictions of the Statistical Model of the Early Stage [4], which treats the creation of the fireball in nucleus–nucleus collisions in a statistical model approach. The model does not attempt a description of the subsequent (hydro-)dynamical evolution of the fireball. First, this section reviews the main assumptions of the originally formulated model and presents results obtained from analytical and numerical calculations as well as comparison to the experimental data available 12 years ago, when the model was formulated. Next, later extensions of the SMES are discussed which address collective flow at freeze-out [16, 22] and event-by-event fluctuations [23, 24]. The subsequent Sec. 4 shows the comparison of the predictions of the model with the most recent experimental results.

3.1. Main assumptions

1. The basic assumption of the SMES is that the production of new degrees of freedom during the early stage of $A+A$ collisions is a statistical process. Thus, formation of all microscopic states allowed by conservation laws is equally probable. As particle creation from energy does not produce net charges, only states with total baryon, flavor and electric charge quantum numbers equal to zero are considered. Presence of the colliding nucleons is assumed to affect the properties of the observed final state only via their interactions with the statistically produced particles during the expansion of the system. This issue is further discussed in point 5 below. Consequently, the properties of the state produced at the early stage are entirely defined by the available energy and the volume in which production takes place. In central $A + A$ collisions this volume is chosen as the Lorentz contracted volume occupied by the colliding nucleons (participant nucleons) from a single nucleus
$$V = \frac{V_0}{\gamma}\,, \tag{1}$$
where $V_0 = \frac{4}{3}\pi r_0^3 A_\mathrm{p}$ and $\gamma = \sqrt{s_{NN}}/(2m_N)$, m_N is the nucleon mass and A_p is the number of participant nucleons from a single nucleus. The r_0 parameter is taken to be 1.30 fm in order to fit the mean baryon density in the nucleus, $\rho_0 = 0.11$ fm^{-3}.

2. Only a fraction, η, of the total energy in $A+A$ collision is transformed into the energy of new degrees of freedom created in the early stage. This is because a part of the energy is carried by the net baryon number

which is conserved during the collision. The released (inelastic) energy can be expressed as

$$E = \eta\,(\sqrt{s_{NN}} - 2m_N)\,A_{\rm p}\,. \tag{2}$$

The parameter η is assumed to be independent of the collision energy and the system size for $A + A$ collisions. The value of η used for the numerical calculations is 0.67 [25].

3. The elementary particles of strong interactions are quarks and gluons. The deconfined state is considered to be composed of u, d and s quarks and the corresponding anti-quarks each with internal number of degrees of freedom equal to 6 (3 color states $\times$ 2 spin states). The contribution of c, b and t quarks can be neglected due to their large masses. The internal number of degrees of freedom for gluons is 16 (8 color states $\times$ 2 spin states). The masses of gluons and non-strange (anti-)quarks are taken to be 0, the strange (anti-)quark mass is taken to be 175 MeV [26]. The properties of equilibrated matter is characterized by an equation of state (EoS). For the case of colored quarks and gluons the model assumes the ideal gas EoS modified by a bag constant B (see, *e.g.*, [3, 27]):

$$p = p^{\rm id} - B\,, \qquad \varepsilon = \varepsilon^{\rm id} + B\,, \tag{3}$$

where p and ε denote pressure and energy density, respectively, and the superscript $^{\rm id}$ marks the quantities for the ideal gas. This equilibrium state is called the Quark Gluon Plasma or Q-state.

4. The model uses an effective parametrization of the confined state, denoted as W-state (White-state). The non-strange degrees of freedom which dominate the entropy production are taken to be massless bosons, as suggested by the original analysis of entropy production in $N + N$ and $A + A$ collisions [28]. Their internal number of degrees of freedom was fitted to the data [28] and appeared to be about 3 times lower than the internal number of effective degrees of freedom in the QGP. The internal number of degrees of freedom for a QGP is $16 + (7/8) \times 36 \cong 48$ and therefore the internal number of non-strange degrees of freedom for low energy collisions is taken to be $48/3 = 16$. The mass of strange degrees of freedom is assumed to be 500 MeV, equal to the kaon mass. The internal number of strange degrees of freedom is estimated to be 14 as suggested by the fit to the strangeness and pion data at the AGS. Also for the W-state the ideal gas EoS is selected. Clearly, this description of the confined state should only be treated as an effective parametrization. The numerical parameters are

fixed by fitting $A+A$ data at the AGS and the parametrization is then used for extrapolation to higher collision energies where the transition between the confined and deconfined state is expected.

5. It is assumed that the matter created at the early stage expands, hadronizes and freezes-out. Within the original SMES formulation these later stage were not modelled. It was, however, postulated that during these stages the total entropy and total number of s and $\overline{s}$ quarks created in the early stage are conserved. The only process which changes the entropy content of the produced matter during the expansion is assumed to be the interaction with the baryonic subsystem. It was argued that this leads to an entropy transfer to baryons which corresponds to the effective absorption of about 0.35 π-mesons per baryon [29]. Thus, the final hadronic state has non-zero baryonic number and electric charge.

3.2. Analytical formulas

In this section the simplified version of the model (massless particles) will be discussed which allows to perform calculations analytically. Subsequently in Sec. 4 quantitative results from numerical calculations using finite masses will be presented and compared to measured data. All chemical potentials have to be equal to zero, as only systems with all conserved charges equal to zero are considered. Thus, the temperature T remains the only independent thermodynamical variable. It is convenient to define the EoS in terms of the pressure function $p = p(T)$ as the entropy and energy densities can be calculated from the thermodynamical relations:

$$s(T) = \frac{dp}{dT}\,, \qquad \varepsilon(T) = T\frac{dp}{dT} - p\,. \tag{4}$$

In the case of an ideal gas the pressure of the particle species j is given by:

$$p^j(T) = \frac{g^j}{2\pi^2}\int\limits_0^\infty k^2 dk \frac{k^2}{3\left(k^2+m_j^2\right)^{1/2}}\left[\exp\left(\frac{\sqrt{k^2+m_j^2}}{T}\right) \pm 1\right]^{-1}\,, \tag{5}$$

where g^j is the internal number of degrees of freedom (degeneracy factor) for the jth species, m_j is the mass of the particle, -1 appears in Eq. (5) for bosons and $+1$ for fermions. The pressure $p(T)$ for an ideal gas of several particle species is additive: $p(T) = \sum_j p^j(T)$. The same is valid for the entropy and energy densities of Eq. (4).

In order to be able to perform analytical calculations of the system entropy and illustrate the model properties, it is assumed that all degrees of

freedom are massless. In this simplified case the pressure Eq. (5) is equal to

$$p^j(T) = \frac{\sigma^j}{3}\, T^4\,, \tag{6}$$

where σ^j is the so-called Stephan–Boltzmann constant, equal to $\pi^2 g^j/30$ for bosons and $\frac{7}{8}\pi^2 g^j/30$ for fermions. The total pressure in the ideal gas of several massless species can then be written as $p(T) = \pi^2 g T^4/90$ with the effective number of degrees of freedom g given by

$$g = g^b + \frac{7}{8} g^f\,, \tag{7}$$

where g^b and g^f are internal degrees of freedom of all bosons and fermions, respectively. The g parameter is taken to be $g_{\rm W}$ for the W-state and $g_{\rm Q}$ for the Q-state, with $g_{\rm Q} > g_{\rm W}$.

The pressure, energy and entropy densities then follow as:

$$p_{\rm W}(T) = \frac{\pi^2 g_{\rm W}}{90} T^4\,, \qquad \varepsilon_{\rm W}(T) = \frac{\pi^2 g_{\rm W}}{30} T^4\,, \qquad s_{\rm W}(T) = \frac{2\pi^2 g_{\rm W}}{45} T^3\,, \tag{8}$$

$$p_{\rm Q}(T) = \frac{\pi^2 g_{\rm Q}}{90} T^4 - B\,, \quad \varepsilon_{\rm Q}(T) = \frac{\pi^2 g_{\rm Q}}{30} T^4 + B\,, \quad s_{\rm Q}(T) = \frac{2\pi^2 g_{\rm Q}}{45} T^3\,, \tag{9}$$

for the pure W- and Q-state, respectively. Note the presence of the non-perturbative bag terms in addition to the ideal quark-gluon gas expressions for the pressure and energy density of the Q-state.

The 1$^{\rm st}$ order phase transition between W- and Q-state is defined by the Gibbs criterion

$$p_{\rm W}(T_{\rm c}) = p_{\rm Q}(T_{\rm c})\,, \tag{10}$$

from which the phase transition temperature can be calculated as

$$T_{\rm c} = \left[\frac{90B}{\pi^2(g_{\rm Q} - g_{\rm W})}\right]^{1/4}\,. \tag{11}$$

At $T = T_{\rm c}$ the system is in the *mixed* phase with the energy and entropy densities given by

$$\varepsilon_{\rm mix} = (1-\xi)\varepsilon^{\rm c}_{\rm W} + \xi\varepsilon^{\rm c}_{\rm Q}\,, \qquad s_{\rm mix} = (1-\xi)s^{\rm c}_{\rm W} + \xi s^{\rm c}_{\rm Q}\,, \tag{12}$$

where $(1-\xi)$ and ξ are the relative volumes occupied by the W- and Q-state, respectively. From Eqs. (8), (9) one finds the energy density discontinuity ('latent heat')

$$\Delta\varepsilon \equiv \varepsilon_{\rm Q}(T_{\rm c}) - \varepsilon_{\rm W}(T_{\rm c}) \equiv \varepsilon^{\rm c}_{\rm Q} - \varepsilon^{\rm c}_{\rm W} = 4B\,. \tag{13}$$

The early stage energy density is an increasing function of the collision energy and is given by (see Eqs. (1), (2))

$$\varepsilon \equiv \frac{E}{V} = \frac{\eta\, \rho_0 \left(\sqrt{s_{NN}} - 2m_N\right) \sqrt{s_{NN}}}{2m_N}\,. \tag{14}$$

There is a remarkable equivalence (see Appendix C of Ref. [4]) of the Gibbs criterion (*i.e.* the pure phase corresponds to the larger pressure $p_{\rm W}$ or $p_{\rm Q}$ and the mixed phase to equal pressures $p_{\rm W} = p_{\rm Q}$) and the maximum entropy criterion,

$$s(\varepsilon) = \max\left\{s_{\rm W}(\varepsilon)\,, s_{\rm Q}(\varepsilon)\,, s_{\rm mix}(\varepsilon)\right\}\,, \tag{15}$$

for an arbitrary EoS $p = p(T)$ with a 1$^{\rm st}$ order phase transition. For $\varepsilon < \varepsilon^{\rm c}_{\rm W}$ or $\varepsilon > \varepsilon^{\rm c}_{\rm Q}$ the system consists of pure W- or Q-state, respectively, with entropy density given by the following equations:

$$s_{\rm W}(\varepsilon) \;=\; \frac{4}{3}\left(\frac{\pi^2 g_{\rm W}}{30}\right)^{1/4} \varepsilon^{3/4}\,, \tag{16}$$

$$s_{\rm Q}(\varepsilon) \;=\; \frac{4}{3}\left(\frac{\pi^2 g_{\rm Q}}{30}\right)^{1/4} (\varepsilon - B)^{3/4}\,. \tag{17}$$

For $\varepsilon^{\rm c}_{\rm W} < \varepsilon < \varepsilon^{\rm c}_{\rm Q}$ the system is in the mixed phase (Eq. 12) and its entropy density can be expressed as:

$$s_{\rm mix}(\varepsilon) = \frac{\varepsilon^{\rm c}_{\rm Q} s^{\rm c}_{\rm W} - \varepsilon^{\rm c}_{\rm W} s^{\rm c}_{\rm Q}}{4B} + \frac{s^{\rm c}_{\rm Q} - s^{\rm c}_{\rm W}}{4B}\varepsilon \equiv a + b\,\varepsilon\,. \tag{18}$$

The ratio of the total entropy of the created state to the number of nucleons participating in $A + A$ collisions is

$$\frac{S}{2A_{\rm p}} = \frac{Vs}{2A_{\rm p}} = \frac{m_N s}{\rho_0 \sqrt{s_{NN}}}\,, \tag{19}$$

and is independent of the number of participant nucleons. The entropy density s in Eq. (19) is given by the general expressions Eq. (15) with ε defined by Eq. (14). For small $\sqrt{s_{NN}}$ the energy density Eq. (14) corresponds to that of the pure W-state and one finds

$$\left(\frac{S}{2A_{\rm p}}\right)_{\rm W} = C g_{\rm W}^{1/4} F\,, \tag{20}$$

where

$$C = \frac{2}{3}\left(\frac{\pi^2 m_N}{15\rho_0}\right)^{1/4} \eta^{3/4}\,, \qquad F = \frac{(\sqrt{s_{NN}} - 2m_N)^{3/4}}{(\sqrt{s_{NN}})^{1/4}}\,. \tag{21}$$

Thus, for low collision energies, where the W-state is created, the entropy per participant nucleon is proportional to F. For high $\sqrt{s_{NN}}$ the pure Q-state is formed and Eq. (19) leads to

$$\left(\frac{S}{2A_{\rm p}}\right)_{\rm Q} = C g_{\rm Q}^{1/4} F \left(1 - \frac{2m_N B}{\eta\rho_0(\sqrt{s_{NN}} - 2m_N)\sqrt{s_{NN}}}\right)^{3/4}$$
$$\cong C g_{\rm Q}^{1/4} F \left(1 - \frac{3m_N B}{2\eta\rho_0 F^4}\right) . \tag{22}$$

For large values of F the entropy per participant nucleon in the Q-state is also proportional to F. The slope is, however, larger than the corresponding slope for the W-state by a factor $(g_{\rm Q}/g_{\rm W})^{1/4}$. In the interval of F in which the mixed phase is formed the energy dependence of the entropy per participant nucleon is given by

$$\left(\frac{S}{2A_{\rm p}}\right)_{\rm mix} = \frac{C_1}{\sqrt{s_{NN}}} + C_2\,(\sqrt{s_{NN}} - 2m_N)\ , \tag{23}$$

where

$$C_1 = \frac{m_N}{\rho_0} a\,, \qquad C_2 = \eta\, b\,. \tag{24}$$

Equation (23) gives approximately a quadratic increase with F of the entropy per participant nucleon in the mixed phase region.

Let us now turn to strangeness. The model defines $g_{\rm W}^{\rm s}$ and $g_{\rm Q}^{\rm s}$ as the numbers of internal degrees of freedom of (anti-)strangeness carriers in the W- and Q-state, respectively. The total entropy of the considered state is given by the sum of entropies of strange and non-strange degrees of freedom. Provided that all particles are massless the fraction of entropy carried by strange (and anti-strange) particles is proportional to the number of strangeness degrees of freedom

$$S_{\rm s} = \frac{g^{\rm s}}{g} S\,. \tag{25}$$

Equation (25) is valid for both W- and Q-state. Note that all degeneracy factors are calculated according to the general relation Eq. (7). For massless particles of the jth species the entropy is proportional to the particle number

$$S_j = 4N_j\,. \tag{26}$$

Thus, the number of strange and anti-strange particles can be expressed as

$$N_{\rm s} + N_{\bar{\rm s}} = \frac{S}{4}\,\frac{g^{\rm s}}{g}\,, \tag{27}$$

and the strangeness to entropy ratio is equal to

$$\frac{N_{\rm s}+N_{\bar{\rm s}}}{S}=\frac{1}{4}\frac{g^{\rm s}}{g}\,. \tag{28}$$

One concludes, therefore, that the strangeness to entropy ratio for the ideal gas of massless particles is dependent only on the ratio of strange to all degrees of freedom, $g^{\rm s}/g$. This ratio is expected to be equal to $g^{\rm s}_{\rm Q}/g_{\rm Q} \cong 0.22$ in the Q-state and $g^{s}_{\rm W}/g_{\rm W} \cong 0.5$ in the W-state. Consequently, the phase transition from the W- to the Q-state should lead to a decrease of the strangeness to entropy ratio by a factor of about 2. This simple picture will be modified because of the large value of the mass of strange degrees of freedom in the W-state ($m^{\rm s}_{\rm W} \cong 500$ MeV) compared to the temperature T. In this case the left-hand side of Eq. (28) is a strongly increasing function of T.

In order to demonstrate properties of the EoS, the ratios of ε/T^4 and p/T^4 are plotted in Fig. 6 as functions of temperature. The bag constant $B = 600$ MeV/fm^3 was adjusted such that the resulting critical temperature $T_{\rm c}$ is equal to 200 MeV.

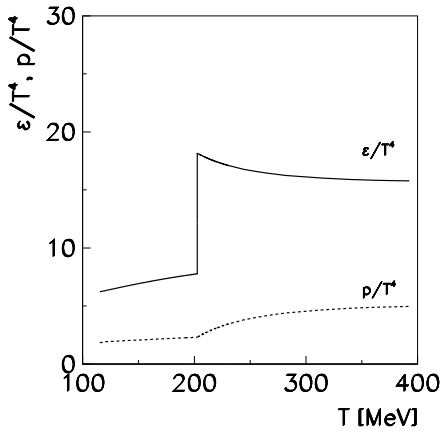

Fig. 6. Energy density and pressure divided by T^4 as a function of temperature T. The bag constant B was adjusted to 600 MeV/fm^3 to obtain a critical temperature $T_{\rm c} = 200$ MeV.

3.3. Quantitative calculations

We next turn to the results from numerical calculations based on the model using finite strangeness carrier masses. For the number of non-strange degrees of freedom $g^{\rm ns}_{\rm Q}$ and $g^{\rm ns}_{\rm W}$ one gets as in the simplified model:

$$g^{\rm ns}_{\rm Q}=2\times 8+\tfrac{7}{8}\times 2\times 2\times 3\times 2=37\,; \qquad g^{\rm ns}_{\rm W}=16\,. \tag{29}$$

The strange degrees of freedom are now considered to have realistic masses $m_{\mathrm{Q}}^{\mathrm{s}}$ and $m_{\mathrm{W}}^{\mathrm{s}}$. Equation (5) is used with

$$g_{\mathrm{Q}}^{\mathrm{s}}=2\times 2\times 3=12\,,\quad m_{\mathrm{Q}}^{\mathrm{s}}\cong 175\,\mathrm{MeV}\,;\quad g_{\mathrm{W}}^{\mathrm{s}}=14\,,\quad m_{\mathrm{W}}^{\mathrm{s}}\cong 500\,\mathrm{MeV}\,. \tag{30}$$

Note that there is no factor $7/8$ in the above expression for $g_{\mathrm{Q}}^{\mathrm{s}}$ as Eq. (5) with Fermi momentum distribution was taken. The contributions of strange degrees of freedom to the entropy and energy densities are calculated using the thermodynamical relations Eq. (4).

A convenient variable to study collision energy dependence is the Fermi–Landau variable F defined in Eq. (21). The dependence of the early stage temperature T (initial temperature of the fireball) on F in the SMES is shown in Fig. 7, left. Outside the transition region T increases approximately linearly with F. Inside the transition region T is constant ($T=T_{\mathrm{c}}=200\,\mathrm{MeV}$). The transition region begins at $F=2.23\ \mathrm{GeV}^{1/2}$ ($p_{\mathrm{LAB}}=30A\,\mathrm{GeV}$) and ends at $F=2.90\ \mathrm{GeV}^{1/2}$ ($p_{\mathrm{LAB}}=64A\,\mathrm{GeV}$). The fraction of the volume occupied by the Q-state, ξ, increases rapidly in the transition region, as shown in Fig. 7, right.

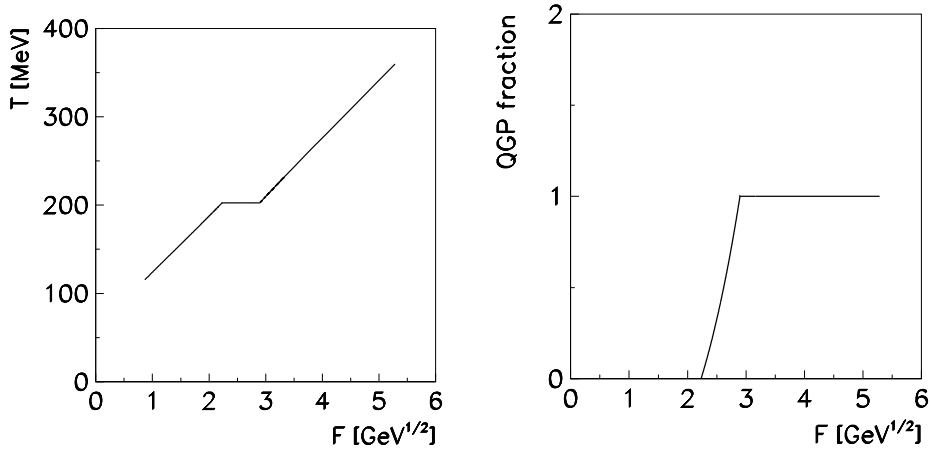

Fig. 7. Left: The early stage (initial) temperature of the fireball as a function of F. Right: The fraction of volume occupied by the QGP as a function of F.

The number of non-strange and strange degrees of freedom and their masses are given by Eqs. (29), (30). They are different in the confined and deconfined phases. Thus, one expects abrupt changes of the pion multiplicity (entropy) (see Fig. 8, left) and the multiplicity of strange particles (see Fig. 9, left) as a function of collision energy in the energy range where a transition from confined to deconfined matter takes place at the early stage of $A+A$ collisions. The comparison of these predictions with experimental results is discussed in Subsecs. 4.1 and 4.2.

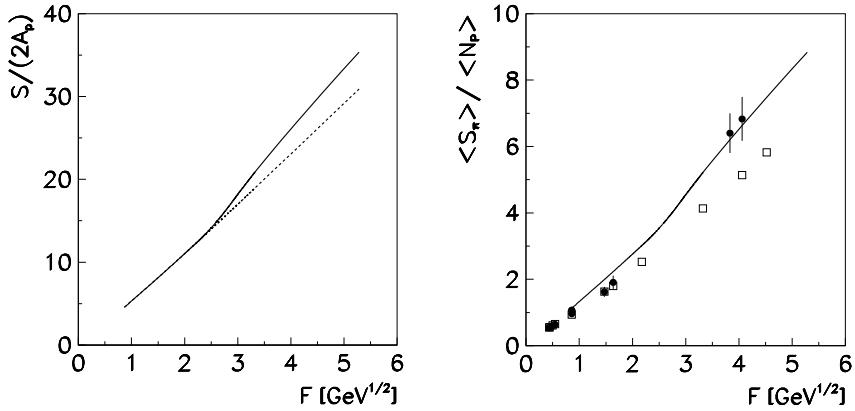

Fig. 8. Left: The entropy per participant nucleon as a function of F (solid line). Dashed line indicates the dependence obtained assuming that there is no transition to the QGP. Right: Ratio of produced entropy in pion units per participant nucleon, $\langle S_\pi \rangle / \langle N_\mathrm{P} \rangle$, as a function of F. Experimental data on central collisions of two identical nuclei are indicated by closed circles. These data correspond to the status of 1998 [10, 11] and should be compared with the model predictions shown by the solid line. The open boxes show results obtained for nucleon–nucleon interactions.

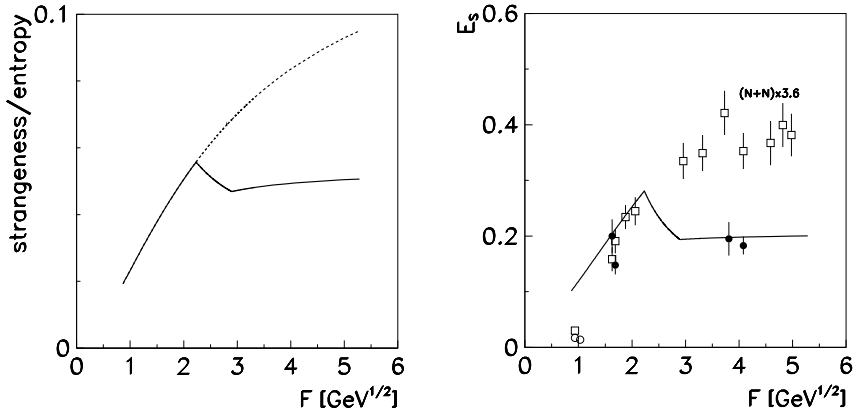

Fig. 9. Left: The ratio of the total number of s and $\overline{s}$ quarks and anti-quarks to the entropy (solid line) as a function of F. The dashed line indicates the corresponding ratio calculated assuming absence of the phase transition to the QGP. Right: The ratio E_s of strange particle to pion production as a function of F. Experimental data on central collisions of two identical nuclei are plotted as closed circles. These data should be compared with the model predictions shown by the solid line. The open boxes show results obtained for nucleon–nucleon interactions, scaled be a factor 3.6 to match $A + A$ data at AGS energy. The plotted data show the status of 1998 as compiled in [10, 11].

3.4. Extensions of the SMES

Several extensions of the SMES were developed over the past 10 years which allow to predict signals of the onset of deconfinement related to the collective flow at freeze-out [16,22] and to event-by-event fluctuations [23,24]. These extensions are briefly presented in this subsection.

3.4.1. Collective flow at freeze-out

The collective flow of matter at freeze-out depends on the properties of the early stage as well as on the expansion dynamics itself. Within the SMES the collision energy dependence of the early stage properties is predicted. In particular, in the energy range in which the mixed phase is created the pressure and temperature are constant and at the end of the mixed phase domain the pressure to energy density ratio reaches its minimum (the softest point of the EoS). From general hydrodynamic considerations this is expected to lead to a reduction of the buildup of transverse [16] and longitudinal [22] collective flow at freeze-out. The corresponding signals are discussed in Subsecs. 4.3 and 4.4.

3.4.2. Event-by-event fluctuations

Up to this point only quantities averaged over many collisions (events) were considered. Next an extension of the SMES is reviewed which leads to predictions of fluctuations from event to event.

The key additional assumption is that when the collision energy is fixed, the energy, which is used for particle production (inelastic energy) can still fluctuate. These dynamical energy fluctuations lead to dynamical fluctuations of macroscopic properties X of the matter, like its entropy and strangeness content [23]. The relation between them is given by the EoS. For example, different values of the energy of the early equilibrium state lead to different, but uniquely determined, entropies. Since the EoS shows an anomalous behavior in the phase transition region, this anomaly should also be visible in the ratio of entropy to energy fluctuations [23].

According to the first and the second principles of thermodynamics the entropy change δS is given as $T\delta S = \delta E + p\delta V$. For central $A+A$ collisions, one expects $\delta V \cong 0$. Within the SMES the ratio of entropy to energy fluctuations can then be calculated and expressed as a simple function of the p/ε ratio [23]

$$R_{\mathrm{e}} \equiv \frac{(\delta S)^2/S^2}{(\delta E)^2/E^2} = \left(1+\frac{p}{\varepsilon}\right)^{-2} . \tag{31}$$

Within the SMES model, confined matter (which is modelled as an ideal gas) is created at the early collision stage below a collision energy of 30 A GeV.

In this domain, the ratio p/ε, and consequently the R_{e} ratio, are approximately independent of the collision energy and equal about $1/3$ and 0.56, respectively. The SMES model assumes that the deconfinement phase transition is of the first order. Thus, there is a mixed phase region, corresponding to the energy interval 30–60 A GeV. At the end of this region the p/ε ratio reaches a minimum (the 'softest point' of the EoS [15]). Thus, in the transition energy range the R_{e} ratio increases and reaches its maximum, $R_{\mathrm{e}} \approx 0.8$, at the end of the transition domain. Further on, in the pure deconfined phase, which is represented by an ideal quark-gluon gas under bag pressure, the p/ε ratio increases and again approaches its asymptotic value $1/3$ at the highest SPS energy of 160 A GeV. The numerically calculated predictions of the SMES are plotted in Fig. 10, left. The early stage energy and entropy fluctuations entering Eq. (31) are not directly observable, however, as argued in Ref. [23], they can be inferred from the experimentally accessible information on the final state energy and multiplicity fluctuations.

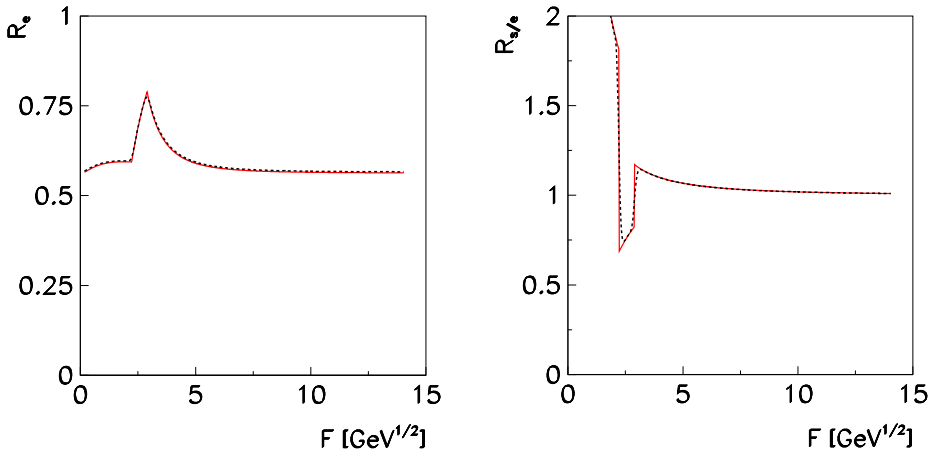

Fig. 10. The collision energy dependence of the fluctuation signals of the onset of the deconfinement calculated within the SMES. Left: The *shark fin* in the ratio of entropy to energy fluctuations R_{e} (31) (see Ref. [23]). Right: The *tooth* structure in the ratio of strangeness and entropy fluctuations $R_{\mathrm{s/e}}$ (33) (see Ref. [24]).

In Ref. [24] the energy dependence of dynamical strangeness fluctuations caused by dynamical energy fluctuations was studied within the SMES model. Defining $\overline{N}_{\mathrm{s}}$ as the total number of strange quark–anti-quark pairs created in an $A + A$ collision one calculates the fluctuation ratio as

$$R_{\mathrm{s}} = \frac{\left(\delta\overline{N}_{\mathrm{s}}\right)^2 \Big/ \overline{N}_{\mathrm{s}}^2}{(\delta E)^2/E^2} \,. \tag{32}$$

For $T \to \infty$ the system is in the QGP phase. Strange (anti-)quarks can be considered as massless and the bag constant can be neglected. Then $\varepsilon \propto T^4$ and $n_s \propto T^3$ and consequently $d\varepsilon/\varepsilon = 4\,dT/T$ and $dn_s/n_s = 3\,dT/T$, which results in $R_s = (3/4)^2 \cong 0.56$. In the confined phase, $T < T_c$, the energy density is still approximately proportional to T^4 due to the dominant contributions of non-strange hadron constituents. However, the dependence of the strangeness density on T is governed by the exponential factor, $n_s \propto \exp(-m_s)$, as $T \ll m_s = m_W^s \cong 500$ MeV. Therefore, at small T one finds $d\varepsilon/\varepsilon = 4\,dT/T$ and $dn_s/n_s = m_s\,dT/T^2$, so that the ratio $R_s = m_s/(4T)$ decreases with T. The strangeness density n_s is small and goes to zero at $T \to 0$, but the fluctuation ratio R_s Eq. (32) is large and increases to infinity in the zero temperature limit. One finds a non-monotonic energy dependence of R_e with a maximum at the boundary between the mixed phase and the QGP [23]. A pronounced minimum-structure is expected in the dependence of R_s on the collision energy [24]. It is located at $\sqrt{s_{NN}} = 7$–12 GeV (30–60 A GeV), where the mixed phase is created at the early stage of $A + A$ collision.

Both entropy and strangeness fluctuation measures, R_e and R_s, show anomalous behavior in the transition region: a maximum is expected for R_e and a minimum for R_s. Consequently, an even stronger anomaly is predicted for the ratio,

$$R_{s/e} \equiv \frac{R_s}{R_e} = \frac{(\delta\overline{N}_s)^2/\overline{N}_s^2}{(\delta\overline{N}_-)^2/\overline{N}_-^2}\,, \tag{33}$$

shown in Fig. 10, right. Experimental measurements of $R_{s/e}$ may be easier than the measurements of R_e and R_s because the ratio $R_{s/e}$ requires measurements of particle multiplicities only, whereas both R_e and R_s involve also measurements of particle energies.

These predictions are discussed in Subsec. 4.5 in the context of existing experimental data.

4. Signals of the onset of deconfinement

Next the predictions of the SMES model reviewed in Sec. 3 will be related to directly measurable quantities and compared with available experimental results. In particular, their significance as evidence for the onset of deconfinement will be discussed in detail.

4.1. The kink

The majority of all particles produced in high energy interactions are pions. Thus, pions carry basic information on the entropy created in the collisions. On the other hand, entropy production should depend on the

form of matter present at the early stage of collisions. Deconfined matter is expected to lead to a final state with higher entropy than that created by confined matter. Consequently, it is natural to expect that the onset of creation of deconfined matter should be signaled by an enhancement of entropy and thus pion production. This simple intuitive argument can be quantified within the SMES.

Equilibration between newly created matter and baryons is assumed to take place during the evolution of the system. It was argued that this equilibration causes transfer of entropy from the produced matter to baryons. The analysis of the pion suppression effect at low collision energies indicates that this transfer corresponds to the effective absorption of about 0.35 pion per participant nucleon [29]. It is further assumed that there are no other processes which change the entropy content of the state produced during the early stage.

For the comparison with the model it is convenient to define the quantity

$$\langle S_\pi \rangle = \langle \pi \rangle + \kappa \left\langle K + \overline{K} \right\rangle + \alpha \langle N_\mathrm{P} \rangle \,, \tag{34}$$

where $\langle \pi \rangle$ is the measured total multiplicity of final state pions and $\langle K + \overline{K} \rangle$ is the multiplicity of kaons and anti-kaons. The factor $\kappa = 1.6$ is the approximate ratio between mean entropy carried by a single kaon to the corresponding pion entropy at chemical freeze-out. The term $\alpha \langle N_\mathrm{P} \rangle$ with $\alpha = 0.35$ is the correction for the discussed partial transfer of the entropy to baryons. The quantity $\langle S_\pi \rangle$ can thus be interpreted as the early stage entropy measured in pion entropy units. The conversion factor between S and $\langle S_\pi \rangle$ is chosen to be 4 ($\approx$ entropy units per pion at chemical freeze-out).

The dependence of the entropy per participant nucleon on F is shown in Fig. 8, left. Outside the transition region the entropy increases approximately proportional to F, but the slope in the Q-state region is larger than the slope in the W-state region.

The number of baryons which take part in the collision ($2A_\mathrm{p}$ in the model calculations) is identified now with the experimentally measured number of participant nucleons, $\langle N_\mathrm{P} \rangle$. The fraction of energy carried by the produced particles is taken to be $\eta = 0.67$ [25] and is assumed to be independent of the size of the colliding nuclei and the collision energy.

The comparison made in 1998 between the ratio $\langle S_\pi \rangle / \langle N_\mathrm{P} \rangle$ calculated from available measurements and the model is shown in Fig. 8, right. The parametrization of the W-state was chosen to fit the AGS data and, therefore, the agreement with low energy $A + A$ data is not surprising. On the other hand, the description of high energy (SPS) results obtained by the NA35 and NA49 collaborations is essentially parameter free.

The pion multiplicity is proportional to the initial entropy, and the $\langle\pi\rangle/\langle N_{\rm P}\rangle$ ratio can thus be calculated outside the transition region as

$$\frac{\langle\pi\rangle}{\langle N_{\rm P}\rangle} \propto g^{1/4}\ F\,, \tag{35}$$

where $g = g_{\rm W}^{\rm ns} = 16$ for the initial state in the confined phase and $g = g_{\rm Q} = 47.5$ for the initial state in the deconfined phase at $T \gg m_{\rm Q}^s$. Therefore, the $\langle\pi\rangle/\langle N_{\rm P}\rangle$ ratio increases linearly with Fermi's energy measure F outside the transition region, and the slope parameter is proportional to $g^{1/4}$ [28]. In the transition region, a steepening of the increase of pion production with energy is predicted, because of the activation of the partonic degrees of freedom.

The recent compilation of data [5] on pion multiplicity produced in central Pb + Pb (Au + Au) collisions and $p + p(\bar{p})$ interactions is shown in Fig. 11 which displays the mean pion multiplicity $\langle\pi\rangle = 1.5\,(\langle\pi^-\rangle + \langle\pi^-\rangle)$ per wounded nucleon as a function of F. The results from $p + p(\bar{p})$ interactions are shown by the open symbols. Up to the top SPS energy the mean pion multiplicity in $p + p$ interactions is approximately proportional to F. A fit of $\langle\pi\rangle/\langle N_{\rm P}\rangle = b\,F$ yields a value of $b \cong 1.063$ GeV$^{-1/2}$. For central Pb + Pb and Au + Au collisions (filled symbols in Fig. 11) the energy dependence is more complicated. Below 40 A GeV ($\sqrt{s_{NN}} = 8.7$ GeV) the ratio $\langle\pi\rangle/\langle N_{\rm P}\rangle$ is lower in $A + A$ collisions than in $p + p(\bar{p})$ interactions (pion suppres-

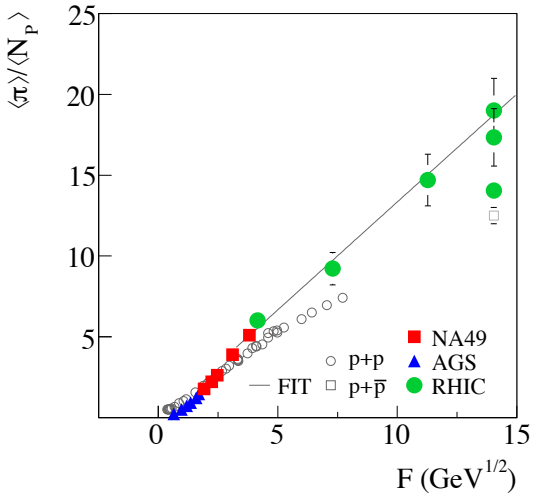

Fig. 11. Energy dependence of the mean pion multiplicity per participant nucleon measured in central Pb + Pb and Au + Au collisions (full symbols), compared to the corresponding results from $p + p(\bar{p})$ reactions (open symbols). The compilation of data is from Ref. [5].

sion) while at higher energies this ratio is larger in $A+A$ collisions than in $p+p(\bar{p})$ interactions (pion enhancement). A linear fit, $\langle\pi\rangle/\langle N_{\mathrm{W}}\rangle = a + b\,F$ for $F < 1.85$ GeV$^{1/2}$ gives $a \cong -0.45$ and $b \cong 1.03$ GeV$^{-1/2}$. The slope parameter fitted in the range $F > 3.5$ GeV$^{1/2}$ is $b \cong 1.33$. This is shown by the solid line in Fig. 11 (the lowest data point at the top RHIC energy was excluded from the fit). Thus, in the region 15–40 A GeV between the highest AGS and the lowest SPS energy the slope increases by a factor of about 1.3. This agrees with the SMES result

$$\left(\frac{g_{\mathrm{Q}}}{g_{\mathrm{W}}^{\mathrm{ns}}}\right)^{1/4} = \left(\frac{47.5}{16}\right)^{1/4} \cong 1.31\,, \tag{36}$$

where the increase is caused by the creation of a transient state of deconfined matter in the early stage of the collisions at energies higher than $\sqrt{s_{NN}} \approx 7.6$ GeV (30 A GeV).

4.2. The horn

The enhanced production of strangeness was considered by many authors as a potential signal of QGP formation [8, 30, 31]. The line of arguments is the following. One estimates that the strangeness equilibration time in the QGP is comparable to the duration of the collision process (< 10 fm/c) and about 10 times shorter than the corresponding equilibration time in hadron matter. It is further assumed that in the early stage of the fireball the strangeness density is much below the equilibrium density, *e.g.*, it is given by the strangeness obtained from the superposition of nucleon–nucleon interactions. Thus, it follows that during the expansion of the matter the strangeness content increases rapidly and approaches its equilibrium value provided matter is in the QGP state. In hadron matter the modification of the initial strangeness content is less significant due to the long equilibration time. This leads to the expectation that strangeness production should rapidly increase when the energy threshold for the production of deconfined matter is crossed from below.

In the SMES the role of strangeness is different. This is because statistical production of particles is postulated and therefore also strange particles are assumed to be produced in equilibrium. Consequently, possible secondary processes do not modify its value. At $T = T_{\mathrm{c}}$ the strangeness density is lower in the QGP than in confined matter. Thus, a suppression of strangeness production is expected to occur when crossing the transition energy range from below. The low level of strangeness production in $N+N$ interactions as compared to the higher strangeness yield per participant nucleon in central $A+A$ collisions (called strangeness enhancement) can be understood as mostly due to the effect of strict strangeness conservation

(canonical suppression) imposed on the strange and anti-strange degrees of freedom [32]. This constraint has an important effect for small statistical systems such as the confined matter in the early stage of $N + N$ collisions.

We are interested in the collision energy region between the AGS and SPS. At 'low' collision energies (when a pure W-state is formed) the strangeness to entropy ratio increases with F. This is due to the fact that the mass of the strange degrees of freedom is significantly higher than the system temperature. At $T = T_c$ the ratio is higher in the W-state than in the Q-state region. Therefore, the ratio decreases in the mixed phase region to the level characteristic for the Q-state. In the Q-state, due to the low mass of strange quarks compared to the system temperature, only a weak dependence of the ratio on F is observed. The F dependence of the strangeness/entropy ratio calculated in the SMES is shown in Fig. 9, left.

The comparison between the model and the data on strangeness production is performed under the assumption that the strangeness content created during the early stage is preserved till the hadronic freeze-out. This simplifies the model calculations by neglecting possible gluon contribution to strangeness production during hadronization of the QGP.

Total strangeness production can be studied (in the AGS and SPS energy range) using the experimental ratio

$$E_s = \frac{\langle \Lambda \rangle + \langle K + \overline{K} \rangle}{\langle \pi \rangle} , \tag{37}$$

where $\langle \Lambda \rangle$ is the mean multiplicity of Λ hyperons (see Appendix B). Within the SMES model E_s of Eq. (37) is calculated as

$$E_s = \frac{(N_s + N_{\bar{s}})/\zeta}{(S - S_s)/4 - \alpha \langle N_P \rangle} , \tag{38}$$

where $\zeta = 1.36$ is the experimentally estimated ratio between total strangeness production and strangeness carried by Λ hyperons and $K + \overline{K}$ mesons [33] and S_s is the fraction of the entropy carried by the strangeness carriers. The comparison between the calculations and the data available in 1998 is shown in Fig. 9, right [4]. The good description of the AGS data is again a consequence of the parametrization of the W-state: $g^s_W = 14$, $m^s_W = 500$ MeV which was based on these data. As in the case of the pion multiplicity, the description of the strangeness results at the SPS (from the NA35 and NA49 collaborations) can be considered as being essentially

parameter free[1]. The agreement with the SPS data is obtained assuming creation of globally equilibrated QGP in the early stage of $A+A$ collisions. The characteristic non-monotonic energy dependence of the E_{s} ratio is a signature of the phase transition.

The entropy and strangeness production in central $A+A$ collisions satisfies well the conditions needed for thermodynamical treatment. Therefore one expects that the measures of the entropy per participant nucleon, $\langle S_\pi\rangle/\langle N_{\mathrm{P}}\rangle$, and the ratio of strangeness to entropy production, E_{s}, are independent of the number of participants for large enough values of $\langle N_{\mathrm{P}}\rangle$.

The energy dependence of the strangeness to entropy production ratio is a crucial signal of deconfinement. The temperature dependence of the multiplicity of a particle is strongly dependent on its mass. In the Boltzmann approximation one finds

$$\langle N_i\rangle = \frac{g^i V}{2\pi^2}\int\limits_0^\infty p^2 dp\, \exp\left(-\frac{\sqrt{p^2+m_i^2}}{T}\right) = \frac{g_i V}{2\pi^2} m_i^2\, T K_2\left(\frac{m_i}{T}\right), \qquad (39)$$

where K_2 is the modified Hankel function. For light particles ($m_{\mathrm{l}}/T \ll 1$) one finds from Eq. (39), $\langle N_{\mathrm{l}}\rangle \propto T^3$, whereas for heavy particles ($m_{\mathrm{h}}/T \gg 1$) Eq. (39) leads to $\langle N_{\mathrm{h}}\rangle \propto T^{3/2}\exp(-m_{\mathrm{h}}/T)$. Within the SMES the strangeness to entropy production ratio increases steeply at low collision energies, when confined matter is produced. This is due to the low temperature at the early stage and the high mass of the carriers of strangeness (the kaon mass). Thus, $m_K \gg T$ and total strangeness production is proportional to $T^{3/2}\exp(-\,m_K/T)$. On the other hand, the total entropy is approximately proportional to T^3. Therefore, the strangeness to pion production ratio is approximately $T^{-3/2}\exp(-m_K/T)$ in the confined phase and strongly increases with the collision energy. When the transition to deconfined matter occurs, the mass of the strangeness carriers is significantly reduced ($m_{\mathrm{s}} \cong 175$ MeV, the strange quark mass). Due to the lower mass ($m_{\mathrm{s}} < T$) the strangeness yield becomes approximately proportional to the entropy (both are proportional to T^3), and the strangeness to entropy (or pion) production ratio becomes independent of energy in the QGP. This leads to a 'jump' in the energy dependence from the larger value for confined matter to the value for deconfined matter. Thus, within the SMES, the

[1] The E_{s} value resulting from a QGP can be estimated in a simple way. Assuming that $m_{\mathrm{s}} = 0$, and neglecting the small ($< 5\%$) effect of pion absorption at the SPS, one gets from Eq. (28) and Eq. (38) $E_{\mathrm{s}} \approx (g_{\mathrm{Q}}^{\mathrm{s}}/1.36)/g_{\mathrm{Q}}^{\mathrm{ns}} \approx 0.21$, where $g_{\mathrm{Q}}^{\mathrm{s}} = (7/8)\times 12$ is the effective number of degrees of freedom of s and $\overline{s}$ quarks and $g_{\mathrm{Q}}^{\mathrm{ns}} = 16+(7/8)\times 24$ is the corresponding number for $u, \overline{u}, d, \overline{d}$ quarks and gluons. Moreover, we use the approximation that the pion entropy at freeze-out is equal to the mean entropy of q, $\overline{q}$ and g in a QGP.

non-monotonic energy dependence of the strangeness to entropy production ratio followed by a plateau at the deconfined value is a direct consequence of the onset of deconfinement taking place at $\sqrt{s_{NN}} \approx 7.6$ GeV (about 30 A GeV) [4].

The E_s ratio was the first observable used to establish the energy dependence of the strangeness to entropy production ratio from the data. This ratio is closely proportional (see Appendix B) to the $\langle K^+ \rangle / \langle \pi^+ \rangle$ ratio, which with time became better measured experimentally. The energy dependence of both ratios is plotted in Fig. 12 for central Pb + Pb (Au + Au) collisions and $p + p$ interactions as function of collision energy.

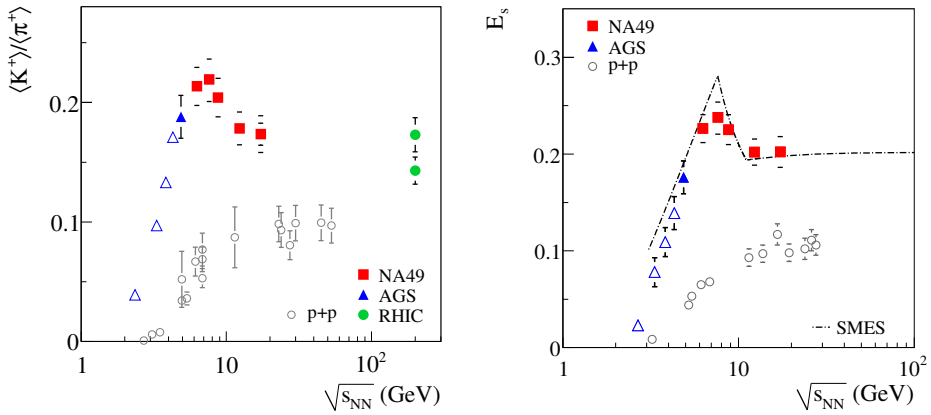

Fig. 12. Left: Energy dependence of the $\langle K^+ \rangle / \langle \pi^+ \rangle$ ratio measured in central Pb + Pb and Au + Au collisions (upper set of symbols) compared to the corresponding results from $p + p$ reactions (lower set of symbols). Right: Energy dependence of the relative strangeness production as measured by the E_s ratio (see text) in central Pb + Pb and Au + Au collisions (upper set of symbols) compared to results from $p+p$ reactions (lower set of symbols). The compilation of data is from Ref. [5]. The dash-dotted line in the figure shows the predictions of the SMES [4].

For $p + p$ interactions the ratios show a monotonic increase with energy. In contrast, a very different behavior is observed for central Pb + Pb (Au + Au) collisions. The steep threshold rise of the ratios characteristic for confined matter changes at high energy into a constant value at the level expected for deconfined matter. In the transition region (at low SPS energies) a sharp maximum is observed caused by the higher strangeness to entropy production ratio in confined matter than in deconfined matter. As seen in Fig. 12 the measured dependence is consistent with that predicted within the SMES [4].

4.3. The step

The energy density at the early stage increases with increasing collision energy. At low and high energies, when a pure confined or deconfined phase is produced, this leads to an increase of the initial temperature and pressure. This, in turn, results in an increase of the transverse expansion of the produced matter and consequently a flattening of the transverse mass spectra of final state hadrons. One may expect an 'anomaly' [14, 15, 16] in the energy dependence of the average hadron transverse momenta in the mixed phase region where the temperature and pressure are approximately constant.

The experimental data on spectra of the transverse mass $m_{\mathrm{T}} = (m^2 + p_{\mathrm{T}}^2)^{1/2}$ are usually parameterized by a simple exponential dependence

$$\frac{dN}{m_{\mathrm{T}} dm_{\mathrm{T}}} \cong C \, \exp\left(-\frac{m_{\mathrm{T}}}{T^*}\right) . \tag{40}$$

The inverse slope parameter T^* is sensitive to both the thermal and collective motion in the transverse direction. Hydrodynamical transverse flow with collective velocity v_{T} modifies the Boltzmann m_{T}-spectrum of hadrons. At low transverse momenta, it leads to the result (T_{kin} is the kinetic freeze-out temperature)

$$T^*_{\mathrm{low}-p_{\mathrm{T}}} \cong T_{\mathrm{kin}} + \tfrac{1}{2} m v_{\mathrm{T}}^2 . \tag{41}$$

Such a linear mass dependence of T^* is supported by the data for hadron spectra at small p_{T}. However, for $p_{\mathrm{T}} \gg m$ the hydrodynamical transverse flow leads to the mass-independent blue-shifted 'temperature'

$$T^*_{\mathrm{high}-p_{\mathrm{T}}} = T_{\mathrm{kin}} \sqrt{\frac{1 + v_{\mathrm{T}}}{1 - v_{\mathrm{T}}}} . \tag{42}$$

Note that a simple exponential fit Eq. (40) neither works for light π-mesons, $T^*_{\mathrm{low}-p_{\mathrm{T}}}(\pi) < T^*_{\mathrm{high}-p_{\mathrm{T}}}(\pi)$, nor for heavy (anti-)protons and (anti-)lambdas, $T^*_{\mathrm{low}-p_{\mathrm{T}}}(p, \Lambda) > T^*_{\mathrm{high}-p_{\mathrm{T}}}(p, \Lambda)$ (see *e.g.*, Refs. [34, 35]).

Kaons are the best suited among measured hadron species for observing the effect of the modification of the EoS due to the onset of deconfinement in hadron transverse momentum spectra. The arguments are the following. First, the kaon m_{T}-spectra are only weakly affected by hadron re-scattering and resonance decays during the post-hydrodynamic hadron cascade at SPS and RHIC energies [34]. Second, a simple one parameter exponential fit Eq. (40) is quite accurate for kaons in central $A+A$ collisions at all energies. This simplifies the analysis of the experimental data. Third, high quality data on m_{T}-spectra of K^+ and K^- mesons in central Pb + Pb (Au + Au) collisions are available over the full range of relevant energies.

The experimental results on the energy dependence of the inverse slope parameter of K^+ and K^- transverse mass spectra for central Pb + Pb (Au + Au) collisions are shown in Fig. 13. The striking features of the data can be summarized and interpreted [16] as follows. The T^* parameter increases strongly with collision energy up to the SPS energy point at $\sqrt{s_{NN}} = 7.6$ GeV (30 A GeV). This is the energy region where the creation of confined matter at the early stage of the collisions is expected. Increasing collision energy leads to an increase of the early stage temperature and pressure. Consequently, the transverse momenta of produced hadrons, measured by the inverse slope parameter, increase with collision energy. This rise is followed by a region of approximately constant value of the T^* parameter in the SPS energy range $\sqrt{s_{NN}} = 7.6$–17.2 GeV (30–158 A GeV), where one expects the transition between confined and deconfined matter with the creation of mixed phases. The resulting modification of the equation of state 'suppresses' the hydrodynamical transverse expansion and leads to the observed plateau structure in the energy dependence of the T^* parameter [16]. At higher energies (RHIC data), T^* again increases with the collision energy. The EoS at the early stage becomes again stiff and the early stage pressure increases with collision energy, resulting in a resumed increase of T^*. As also shown in Fig. 13 the parameter T^* in $p + p$ interactions appears to increase smoothly and does not show the step-like structure.

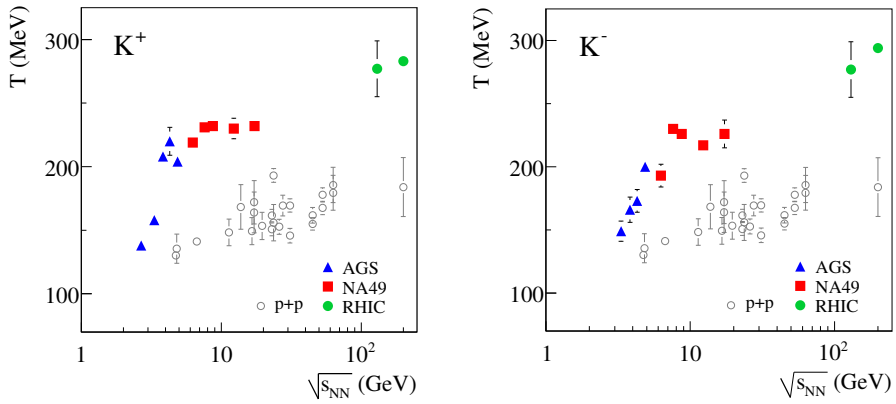

Fig. 13. Energy dependence of the inverse slope parameter T^* of the transverse mass spectra of K^+ (left) and K^- mesons (right) measured at mid-rapidity in central Pb + Pb and Au + Au collisions. The $K^\pm$ slope parameters are compared to those from p+p reactions (open circles). The compilation of data is from Ref. [5].

For the transverse mass spectra of pions and protons the inverse slope parameter depends on the transverse mass interval used in the fit. The mean transverse mass $\langle m_{\mathrm{T}} \rangle$ provides an alternative characterization of the

m_{T}-spectra. The energy dependence of $\langle m_{\mathrm{T}}\rangle - m$ for pions, kaons and (anti-)protons is shown in Fig. 14. These results demonstrate that the approximate energy independence of $\langle m_{\mathrm{T}}\rangle - m$ in the SPS energy range is a common feature for all abundantly produced particle species.

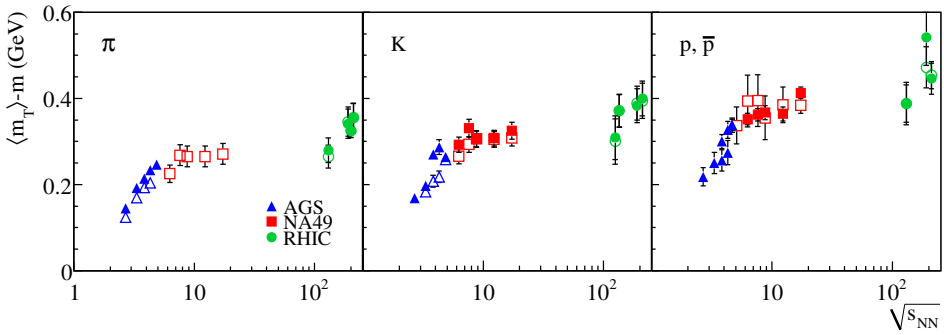

Fig. 14. Energy dependence of the mean transverse mass, $\langle m_{\mathrm{T}}\rangle - m$, measured at mid-rapidity in central Pb + Pb and Au + Au collisions for $\pi^{\pm}$ (left), $K^{\pm}$ (middle), and p and $\bar{p}$ (right). Results for positively (negatively) charged hadrons are shown by full (open) symbols. The compilation of data is from Ref. [5].

4.4. The dale

This subsection summarizes the analysis of Ref. [22] of the longitudinal pion spectra within Landau's hydrodynamical model [36, 37]. The interest in this model was revived by the remarkable observation that the rapidity distributions at all investigated energies can be well described by a single Gaussian (see [38] and references therein). Moreover, the energy dependence of the width can also be described reasonably well by the same model.

The main physics assumptions of Landau's picture are as follows. The collision of two Lorentz-contracted nuclei leads to a complete stopping of the colliding nuclei and full thermalization of the created hadronic matter. This establishes the volume and energy density for the initial conditions of hydrodynamic expansion at each collision energy. Assuming for simplicity the equation of state in the form $p = c_{\mathrm{s}}^2\varepsilon$ (c_{s} denotes the speed of sound, and $c_{\mathrm{s}}^2 = 1/3$ for an ideal massless particle gas) the pion rapidity spectrum is given by [39, 40]

$$\frac{dn}{dy} = \frac{K s_{NN}^{1/4}}{\sqrt{2\pi\sigma_y^2}} \exp\left(-\frac{y^2}{2\sigma_y^2}\right) \tag{43}$$

with

$$\sigma_y^2 = \frac{8}{3}\frac{c_{\mathrm{s}}^2}{1-c_{\mathrm{s}}^4} \ln\left(\sqrt{s_{NN}}/2m_{\mathrm{N}}\right) , \tag{44}$$

where K is a normalization factor converting entropy to pion density[2]. The above prediction was compared with the experimental data on rapidity distributions of negatively charged pions produced in central Pb + Pb (Au + Au) collisions at various energies. Figure 15, left shows the measured width σ_y of the rapidity spectra [41, 38, 42, 43] as a function of the beam rapidity. The full line shows a linear fit through the data points. The dotted line indicates the Landau model predictions with $c_s^2 = 1/3$.

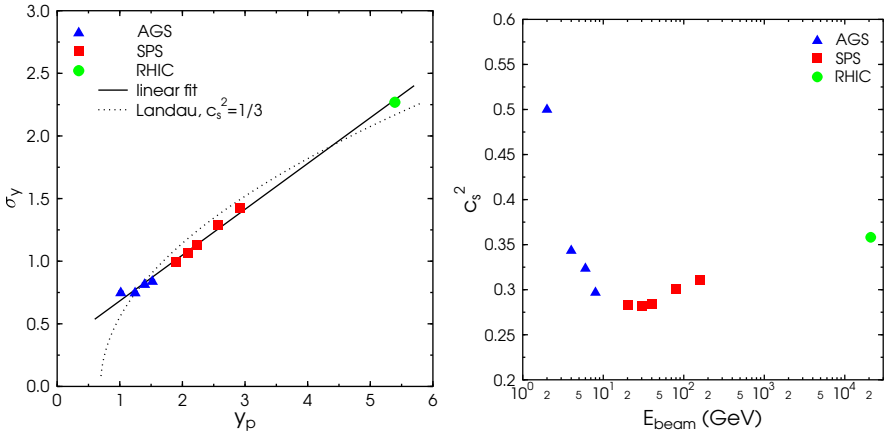

Fig. 15. Comparison of the Landau hydrodynamic model with rapidity distributions of charged particles [22]. Left: The root mean square width σ_y of the rapidity distributions of negatively charged pions in central Pb + Pb (Au + Au) reactions as a function of the beam rapidity y_p. The dotted line indicates the Landau model prediction with $c_s^2 = 1/3$, while the full line shows a linear fit through the data points. Data (full symbols) are taken from [41, 38, 42, 43]. The statistical errors given by the experiments are smaller than the symbol sizes. Systematic errors are not available. Right: Speed of sound as a function of beam energy for central Pb + Pb (Au + Au) reactions as extracted from the data using Eq. (45). The statistical errors (not shown) are smaller than 3%.

The model only roughly reproduces the measured dependence. At low AGS energies and at the top RHIC energy, the experimental points are under-predicted, while in the SPS energy regime Landau's model over-predicts the width of the rapidity distributions.

[2] There are two issues related to derivation of Eq. (44) which need clarification by future study. First, Eq. (44) is obtained assuming that c_s depends only on the early stage energy density and its dependence on decreasing energy density during expansion is neglected. Second, the Landau model assumes stopping and thermalization of the total energy in the c.m. system, whereas only a fraction of the inelastic energy is stopped and thermalized in the SMES model.

These deviations can be attributed to the changes in the EoS, which can be effectively parameterized by allowing the speed of sound to be dependent on collision energy. By inverting Eq. (44) one can express c_{s}^2 in the medium as a function of the measured width of the rapidity distribution

$$c_{\mathrm{s}}^2 = -\frac{4}{3}\frac{\ln(\sqrt{s_{NN}}/2m_p)}{\sigma_y^2} + \sqrt{\left[\frac{4}{3}\frac{\ln(\sqrt{s_{NN}}/2m_N)}{\sigma_y^2}\right]^2 + 1}\,. \tag{45}$$

The energy dependence of the sound velocities extracted from the data using Eq. (45) is presented in Fig. 15, right. The sound velocities exhibit a clear minimum (usually called the softest point) around a beam energy of $\sqrt{s_{NN}} = 7.6$ GeV (30 A GeV).

As discussed previously the weakening of the transverse and longitudinal expansion is expected within the SMES at low SPS energies due to the onset of deconfinement which softens the EoS at the early stage. Generally, a softening of the equation of state was predicted as a signal for the mixed phase at the transition energy from hadronic to partonic matter [44, 45, 46]. Therefore, we conclude that the data on rapidity spectra of negatively charged pions are indeed compatible with the assumption of the onset of deconfinement at the low SPS energies.

4.5. The shark fin and the tooth

As discussed in Subsec. 3.4 the event-by-event fluctuations of the energy used for particle production should lead to fluctuations which are sensitive to the onset of deconfinement.

The NA49 Collaboration looked for the *shark fin* structure in the energy dependence of the scaled variance of multiplicity distributions in central Pb + Pb collisions [47]. The predicted [23] increase of the scaled variance of multiplicity distribution in the NA49 acceptance by about 0.01 due to the onset of deconfinement is smaller than the systematic error on the measurement. Therefore these data can neither support nor disprove the *shark fin* prediction.

The *tooth* structure in the energy dependence of $R_{\mathrm{s/e}}$ shown in Fig. 10, right might be seen in the event-by-event fluctuations of the K/π ratio. The energy dependence of the fluctuations of this ratio in central Pb + Pb collisions was studied by NA49 using the so-called σ_{dyn} measure [48]. The 'dynamical' K/π fluctuations increase significantly with decreasing energy below 40 A GeV. It is unclear whether this increase is related to the rapid increase of the $R_{\mathrm{s/e}}$ measure predicted due to the onset of deconfinement at energies below 30 A GeV.

5. Alternative approaches

Several other analyzes of the energy dependence of hadron production properties in central Pb + Pb and Au + Au collisions within various theoretical approaches support the hypothesis that the onset of deconfinement is located at low SPS energies. In particular such a result was obtained from studies of hadron yields within a non-equilibrium hadron gas model [49] and from an analysis of the time evolution of the relative strangeness yield using the momentum integrated Boltzmann equation [50]. Moreover, a simultaneous analysis of the two-pion correlation function and the transverse mass spectra found a plateau in the averaged phase-space density at SPS energies which may be associated with the onset of deconfinement [51].

Recently a parity violating signal was observed in three-particle azimuthal correlations at RHIC [52]. Such an effect was predicted [53] since metastable domains may form in a QGP where parity and time-reversal symmetries are locally violated. The effect is expected to disappear when no QGP is produced in the collisions. It can therefore serve as an another indicator for the onset of deconfinement.

Numerous models have been developed to explain hadron production in reactions of heavy nuclei without explicitly invoking a transient QGP phase. The simplest one is the statistical hadron gas model [54] which assumes that the hadrochemical freeze-out creates a hadron gas in equilibrium. The temperature, the baryon chemical potential, and the hadronization volume are free parameters of the model and are fitted to the data at each energy. In this formulation, the hadron gas model cannot make any prediction about the energy dependence of hadron production so that an extension of the model was proposed, in which the values of the temperature and baryon chemical potential evolve smoothly with collision energy [55]. By construction (fit to the energy dependence), the prevailing trend in the data is reproduced by the model but important details are not, *e.g.*, the decrease of the $\langle K^+\rangle/\langle\pi^+\rangle$ ratio between $\sqrt{s_{NN}} = 7.6$ and 12.3 GeV (30 and 80 A GeV) is not well described. The measured ratio of strangeness to pion yield in central Pb + Pb collisions at $\sqrt{s_{NN}} = 17.2$ GeV (158 A GeV) is about 25% lower than the expectation for the fully equilibrated hadron gas [55, 56]. Two strategies are followed in order to improve the quality of the hadron gas model fits. First, additional parameters have been introduced which allow for deviations from equilibrium [57, 58, 49]. Obviously the non-equilibrium hadron gas models [57, 58, 49] with all the parameters fitted separately to the data at each energy describe the experimental results significantly better. Secondly, the equilibrium model was extended to include hypothetical high mass resonance states [59]. Again by adding additional free parameters (mass dependence of the resonance state density and their branching ratios) the fit quality can

be improved. Interestingly, the energy dependence of the parameters obtained within the extended hadron gas models is interpreted [49, 59] as an indication for the onset of deconfinement at $\sqrt{s_{NN}} \approx 7.6$ GeV (30 A GeV).

Dynamical models of nucleus–nucleus collisions, such as RQMD [60], UrQMD [61] and HSD [62] treat the initial nucleon–nucleon interactions within a string-hadronic framework. In addition, these models include effects such as string–string interactions and hadronic re-scattering which are expected to be relevant in nucleus–nucleus collisions. RQMD [60, 63], UrQMD [61, 64, 65] and HSD [65] models, like the hadron gas model, fail to describe the rapid change of hadron production properties with collision energy in the low SPS energy range.

It was shown that the maximum in relative strangeness production can be reproduced by invoking an unusually long lifetime of the fireball at low SPS energies which decreases with collision energy [66]. This assumption is however difficult to justify by dynamical models of the collision process [61, 62], and conflicts with the measured energy dependence of the two-pion correlation function [67, 68].

The step-like structure in the energy dependence of the inverse slope parameter of the transverse mass spectra was obtained within the hydrodynamical model by introduction of a rapid change of the freeze-out conditions at low SPS energies [69]. However, this assumption does not explain the increase of the inverse slope parameter suggested by the RHIC results.

In summary, one is led to conclude that models which do not invoke the onset of deconfinement at low SPS energies cannot explain comprehensively and consistently the energy dependence of hadron production properties in central Pb + Pb (Au + Au) collisions.

6. Open problems

Open questions related to the onset of deconfinement are discussed in this section. First the theoretical questions are addressed, then the experimental issues are discussed.

6.1. Theoretical problems

Quantum chromodynamics, the commonly accepted theory of strong interactions, was developed to model the interactions of quarks and gluons as well as their color neutral composites, the hadrons. Thus, in principle, this theory should be able to predict whether and via which observables the onset of deconfinement can be experimentally observed in nucleus–nucleus collisions. In QCD the strength of the strong force between two quarks increases with their distance. This property of the theory has as a consequence

that, in general, predictions are either very difficult or impossible to calculate. Presently, there are no quantitative QCD predictions yet concerning the onset of deconfinement in nucleus–nucleus collisions.

The SMES model [4] assumes statistical particle production at the early stage of nucleus–nucleus collisions. The data on nucleus–nucleus collisions at RHIC, in particular results on anisotropic flow, seem to require a large degree of equilibration at the early stage of collisions [70]. Thus, the assumption of statistical particle production received independent experimental support.

The additional assumptions of the SMES, which lead to the *kink* and *horn* predictions, concern entropy and strangeness conservation during expansion and freeze-out. In fact, the model predictions remain at least qualitatively unchanged if one assumes an approximate proportionality of the final state entropy and strangeness to their early stage values. There is no easy way to prove or disprove these weaker requirements.

The predictions concerning the *step* and *dale* require assumptions concerning the equation of state of strongly interacting matter. In particular, they rely on a general feature of the EoS, *i.e.* the existence of the softest point when the transition between QGP and confined matter occurs. Thus, the qualitative predictions are independent of the nature of the transition (*e.g.*, cross-over or 1^{st} order phase transition, full or partial energy stopping and thermalization). However, the quantitative predictions are sensitive and a consistent description of the hydrodynamical evolution has not been achieved yet. In particular, the bag model equation of state with a 1^{st} order phase transition to hadron gas leads to a significant over-prediction of transverse flow [71]. Further studies are needed.

The predictions concerning the *tooth* and *shark fin* are derived assuming that the early stage volume fluctuations can be neglected for central collisions. It is unclear, to which extent this condition is consistent with recent attempts to describe multiplicity distributions and high transverse momentum spectra in $p+p$ interactions by a statistical model with volume fluctuations [72]. Further studies are needed.

6.2. Experimental issues

The experimental results indicating the onset of deconfinement were obtained mainly by the NA49 experiment at the CERN SPS. Clearly, a confirmation of these measurements is necessary.

A beam energy scan program at the BNL RHIC has recently started. Pilot results at $\sqrt{s_{NN}} = 9.2$ and 20 GeV are in agreement with the corresponding NA49 data [73]. New RHIC data being taken by the STAR experiment in 2010 will allow a more conclusive verification of the NA49 results.

At the CERN SPS the new experiment NA61 started a two-dimensional system size and beam energy scan in 2009, which will continue over the next 4 years. The measurements aim to verify the existence of the onset of deconfinement in collisions of medium size nuclei. Moreover, they will allow to study the expected disappearance of the signals in collisions of light nuclei.

7. Summary and conclusions

In this review we present the experimental and theoretical status of the evidence for the threshold of quark-gluon plasma creation in high energy nucleus–nucleus interactions. The location in energy of this so-called onset of deconfinement, as well as key experimental signals were predicted by the statistical model of the early stage of the collision process [4]. These signals were searched for and observed within the energy scan program of the NA49 Collaboration at the CERN SPS. Together with measurements at lower (LBL, JINR, SIS, BNL AGS) and higher (BNL RHIC) energies the properties of hadron production in heavy ion collisions were established in a broad energy range. Their energy dependence led to the conclusion that the predicted signals of the onset of deconfinement appear in a common energy domain covered by the SPS at CERN. These features of the data serve as strong experimental evidence for the existence of the onset of deconfinement and thus for the quark-gluon plasma itself.

Quantitative model predictions, discussed in this review, are derived within the statistical approach to particle production in high energy collisions. The use of this approach has a two-fold justification. First, it naturally includes the concept of phases of strongly interacting matter and the transition between them. Second, it is successful in describing numerous features of the experimental data. The relation between the statistical approach and the commonly accepted theory of strong interactions, QCD, remains unclear. This is because QCD is difficult or impossible to evaluate in the energy region relevant for multi-particle production in general and for the phase transitions of strongly interacting matter in particular.

New experimental programs have started at the CERN SPS and BNL RHIC which are devoted to the study of nucleus–nucleus collisions in the energy region where the NA49 experiment found evidence for the onset of deconfinement. The STAR experiment at RHIC will provide a necessary confirmation of these results. The new CERN experiment NA61 will address the questions how this observed phenomenon depends on the volume of matter and what the properties of the transition region are.

Appendix A

Strangeness enhancement and J/ψ suppression

The idea of strangeness enhancement as a quark-gluon plasma signal in nucleus–nucleus ($A+A$) collisions was formulated a long time ago [8]. It was based on the estimate that the strangeness equilibration time in the QGP is of the same order ($\approx$ 10 fm/c) as the expected life time of the fireball formed in $A+A$ collisions. Thus, in the case of QGP creation strangeness is expected to approach its QGP equilibrium value. This equilibrium value is significantly higher than the level of strangeness production in nucleon–nucleon ($N+N$) collisions. Strangeness production in secondary hadronic interactions was estimated to be negligibly small. Therefore, if QGP is not formed, strangeness yields would be expected to be much lower than those predicted by equilibrium QGP calculations. Thus, at that time a simple and elegant signature of QGP creation appeared: a transition to QGP should be signaled by an increase of the strangeness production level to the QGP equilibrium value.

The actual study has been done in the following way. The strangeness to pion ratio quantified by the ratios,

$$E_{\mathrm{s}} = \frac{\langle \Lambda \rangle + \langle K + \overline{K} \rangle}{\langle \pi \rangle} \qquad \text{or} \qquad \frac{\langle K^+ \rangle}{\langle \pi^+ \rangle}\,, \tag{A.1}$$

was measured and analyzed. One expected that the ratios should increase *strongly* in $A+A$ collisions if the QGP was formed. To reveal the specific increase of the strangeness/pion ratio in $A+A$ collisions due to QGP formation the strangeness enhancement factor was introduced

$$R_{\mathrm{s}}\left(\sqrt{s_{NN}}\right) \equiv \frac{E_{\mathrm{s}}^{AA}\left(\sqrt{s_{NN}}\right)}{E_{\mathrm{s}}^{NN}\left(\sqrt{s_{NN}}\right)} \approx \frac{\left(\langle K^+ \rangle / \langle \pi^+ \rangle\right)_{AA}}{\left(\langle K^+ \rangle / \langle \pi^+ \rangle\right)_{NN}}\,, \tag{A.2}$$

where superscripts ^{AA} and ^{NN} correspond respectively to $A+A$ and $N+N$ collisions at the same $N+N$ c.m. energy $\sqrt{s_{NN}}$. The confrontation of this expectation with data was for the first time possible in 1988 when results from ^{32}S and ^{28}Si beams at the SPS and the AGS became available. Experiment NA35 reported that in central S + S collisions at 200 A GeV the strangeness to pion ratio is indeed about 2 times higher than in $N+N$ interactions at the same energy per nucleon [74]. But an even larger enhancement (R_{s} is about 5) was measured by E802 in Si + A collisions at the AGS. The data on central Au + Au collisions at low AGS energies 2–10 A GeV completed the picture: strangeness enhancement is observed at all energies, and it is stronger at lower energies, *i.e.* the ratio R_{s} Eq. (A.2) *increases* monotonically with *decreasing* $\sqrt{s_{NN}}$. Figure 16 shows a compilation of recent data [75].

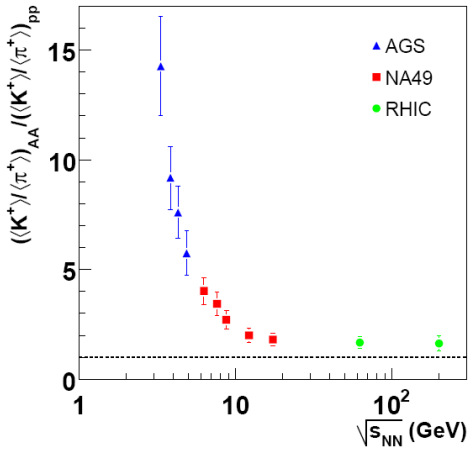

Fig. 16. Energy dependence of strangeness enhancement in central Pb + Pb (Au + Au) collisions [75].

Moreover, the enhancement factor R_s Eq. (A.2) should evidently go to infinity at the threshold energy of strange hadron production in $N + N$ collisions. At low AGS energies one does not expect the creation of a QGP and therefore the substantial strangeness enhancement is clearly of a different origin. The low level of strangeness production in $p + p$ interactions as compared to the strangeness yield in central $A+A$ collisions can be understood to a large extent in the statistical model as due to the effect of exact strangeness conservation. The canonical ensemble treatment of strangeness conservation leads to additional suppression factors imposed on strange hadron production in small systems such as created in $p+p$ collisions. In any case, the AGS measurements indicating a strangeness enhancement R_s larger than that at the SPS show clearly that the simple concept of strangeness enhancement as a signal of QGP production does not work.

The standard picture of J/ψ production in collisions of hadrons and nuclei assumes a two step process: the creation of a $c\bar{c}$ pair in hard parton collisions at the very early stage of the reaction and subsequent formation of a bound charmonium state. It was proposed [9] to use the J/ψ as a probe for deconfinement in the study of $A + A$ collisions. The argument was that in a QGP color screening dissolves initially created J/ψ mesons into c and $\bar{c}$ quarks which at hadronization form open charm hadrons. As the initial yield of J/ψ is believed to have the same A-dependence as the yield of Dell–Yan lepton pairs, the measurement of a weaker A-dependence of the final J/ψ yield (J/ψ suppression) would signal charmonium absorption and therefore creation of QGP.

Production of charmonium states J/ψ and ψ' was measured in $A+A$ collisions at the CERN SPS over a period of 15 years by the NA38, NA50 and NA60 collaborations [76]. The A-dependence of J/ψ production in $p+A$ is weaker than A^1 (approximately $A^{0.9}$). It was suggested that this J/ψ suppression is due to absorption on nucleons in the target nucleus. The data on oxygen and sulfur collisions on nuclei at 200 A GeV also indicated considerable suppression. To improve the fit of the data a new source of J/ψ absorption was introduced: the absorption on hadronic secondaries ('co-movers'). Finally, in central Pb + Pb collisions at 158 A GeV the measured suppression was found to be significantly stronger than expected in the models including nuclear and co-mover suppression. This 'anomalous' J/ψ suppression was interpreted as evidence of QGP creation in Pb + Pb collisions at the CERN SPS. The uncertainties in estimates of the J/ψ absorption by target nucleons and co-movers make J/ψ suppression a problematic QGP signal. An essential part of the J/ψ yield comes from decays of excited charmonium states like ψ' and χ. All of them have different melting temperatures and absorption cross-sections.

Alternative approaches have been developed, namely the statistical [77] and the statistical coalescence [78, 79] models of J/ψ production, which reproduce the A-dependence of the J/ψ yield at SPS energies reasonably well. They are based on different physics pictures than the one leading to J/ψ suppression as the signal of quark-gluon plasma creation. Specifically, the statistical model [77] assumes statistical production of J/ψ mesons at hadronization, whereas in the coalescence model statistical coalescence of c and $\overline{c}$ quarks at hadronization is assumed [78, 79]. In both models the J/ψ yield is neither related to the J/ψ suppression in the hadron gas nor in the quark-gluon plasma.

Appendix B

Main carriers of s and $\bar{s}$ quarks

The distribution of s and $\bar{s}$ quarks among the most abundantly produced hadrons is considered here for the case of nucleus–nucleus collisions at the SPS energies. The sketch presented in Fig. 17 illustrates the following discussion.

The colliding nuclei have net numbers of s and $\bar{s}$ quarks equal to zero. As strangeness is conserved in strong interactions the numbers of s and $\bar{s}$ quarks in the final state have to be equal.

Kaons are the lightest strange hadrons. The isospin partners K^+ and K^0 mesons carry $\bar{s}$ quarks, whereas K^- and $\bar{K}^0$ carry s quarks. The (approximate) symmetry of the initial state and isospin conservation in strong

interactions imply that:

$$\langle K^+ \rangle \approx \langle K^0 \rangle \tag{B.1}$$

and

$$\langle K^- \rangle \approx \langle \bar{K}^0 \rangle \ . \tag{B.2}$$

The $\bar{s}$-quarks are also carried by the lightest anti-baryon, $\bar{\Lambda}$. Its fraction is however small (less than 5%) at the AGS and SPS energies due to suppression of the anti-baryon yield by the high net-baryon density. Consequently, K^+ and K^0 mesons carry each about half of all the anti-strange quarks produced in $A + A$ collisions at AGS and SPS energies. Thus, their yields are nearly proportional to the total number of produced s and $\bar{s}$ quarks.

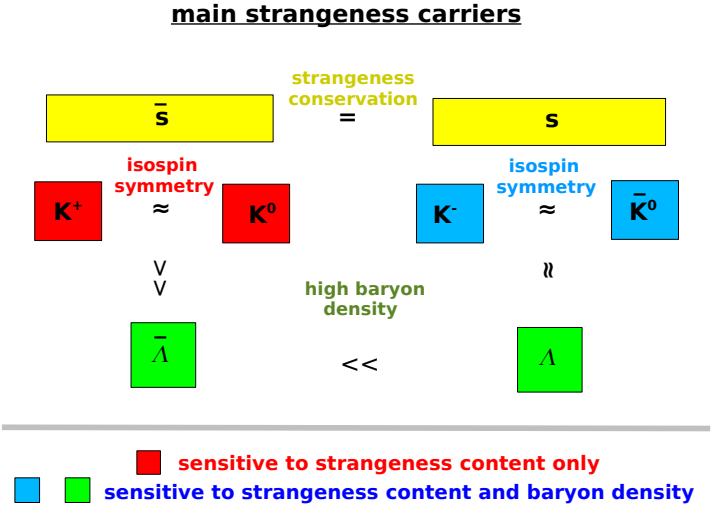

Fig. 17. Main carriers of s and $\bar{s}$ quarks. K^- and $\bar{K}^0$ as well as Λ and $\bar{\Lambda}$ yields are sensitive to the strangeness content and baryon density. K^+ and K^0 yields are sensitive mainly to strangeness content.

This is not the case for K^- and $\bar{K}^0$ mesons. A significant fraction of s-quarks (about 50% in central Pb + Pb collisions at 158 A GeV) is carried by hyperons. In addition, this fraction strongly depends on collision energy. Consequently, the fraction of s-quarks carried by anti-kaons, K^- and $\overline{K}^0$, is also dependent on collision energy and cannot be used easily to quantify strangeness production. In the E_{s} ratio all main carriers of strange and anti-strange quarks are included. The neglected contribution of $\overline{\Lambda}$ and other hyperons and anti-hyperons is about 10% at SPS energies. Both the $\langle K^+ \rangle / \langle \pi^+ \rangle$ and E_{s} ratios are approximately, within 5% at SPS energies, proportional to the ratio of total multiplicity of s and $\bar{s}$ quarks to the multiplicity of pions. It should be noted that the $\langle K^+ \rangle / \langle \pi^+ \rangle$ ratio is expected

to be similar (within about 10%) for $p+p$, $n+p$, and $n+n$ interactions at 158 A GeV, whereas the E_s ratio is independent of the isospin of nucleon–nucleon interactions.

Appendix C

Onset of deconfinement and critical point

This appendix discusses relations between the onset of deconfinement, the critical point of strongly interacting matter and the possibilities of their experimental study in relativistic nucleus–nucleus collisions. The two sketches presented in Fig. 18 should help to understand the basic ideas.

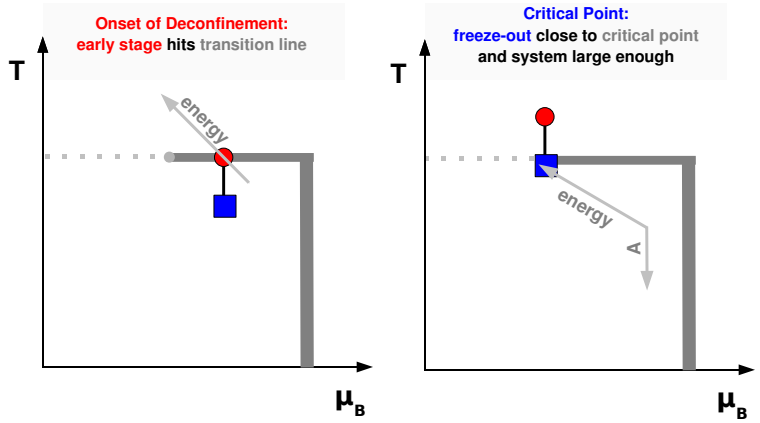

Fig. 18. Onset of deconfinement and critical point.

The onset of deconfinement refers to the beginning of the creation of a deconfined state of strongly interacting matter (ultimately a quark-gluon plasma) at the early stage of nucleus–nucleus collisions when increasing the collision energy. With increasing collision energy the energy density of matter created at the early stage of $A+A$ collisions increases. Thus, if there are two phases[3] of matter separated by the transition region (solid and dotted lines) as indicated in Fig. 18, left the early stage (the red point) first has to hit and then move above the transition region. Therefore, the existence of the onset of deconfinement is the most straightforward consequence of the existence of two phases of strongly interacting matter, *i.e.* confined matter and QGP. The experimental observation of the onset of deconfinement

[3] The discussed two phase diagram is the simplest one which allows to introduce the concepts of the onset of deconfinement and the transition region. There are numerous suggestions of phase diagrams with a significantly richer structure (see *e.g.*, Ref. [80]).

required a one dimensional scan in collision energy with heavy ions as performed by NA49. All signals of the onset of deconfinement discussed in this paper relate to the difference in properties of confined matter and QGP. They are not sensitive to the structure of the transition region.

Discovery of the onset of deconfinement implies the existence of QGP and of a transition region between confined and QGP phases. Numerous possibilities concerning the structure of the transition region are under discussion (see *e.g.*, Ref. [81]). The most popular one [82], sketched in Fig. 18, claims that a 1$^{\text{st}}$ order phase transition (thick gray line) separates both phases in the high baryonic chemical potential domain. In the low baryonic chemical potential domain a rapid crossover is expected (dotted line). The end point of the 1$^{\text{st}}$ order phase transition line is the critical point.

The characteristic signatures of the critical point can be observed if the freeze-out point (blue square in Fig. 18, right) is located close to the critical point. The analysis of the existing experimental data [58] indicates that the location of the freeze-out point in the phase diagram depends on the collision energy and the mass of the colliding nuclei. This dependence is schematically indicated in Fig. 18, right. Thus, the experimental search for the critical point requires a two-dimensional scan in collision energy and size of the colliding nuclei. The NA61 experiment [17, 18] at the CERN SPS started this scan in 2009. It should be completed within several years. Note, that a two dimensional scan is actually required for any study of the structure of the transition region, independent of the hypothesis tested.

The transition region can be studied experimentally in nucleus–nucleus collisions only at T, μ_B values which correspond to collision energies higher than the energy of the onset of deconfinement. This important conclusion is easy to understand when looking at Fig. 18. Signals of the critical point can be observed provided the freeze-out point is close to it (see Fig. 18, right). On the other hand, by definition the critical point is located on the transition line. Furthermore, the energy density at the early stage of the collision is, of course, higher than the energy density at freeze-out. Thus, the condition that the freeze-out point is near the critical point implies that the early stage of the system is above (or on) the transition line. This in turn means that the optimal energy range for the search for the critical point lies above the energy of the onset of deconfinement (see Fig. 18, left). This general condition limits the search for the critical point to the collision energy range $E_{\text{LAB}} > 30\,A\,\text{GeV}$.

REFERENCES

[1] D.D. Ivanenko, D.F. Kurdgelaidze, *Astrophysics* **1**, 251 (1965) [*Astrofiz.* **1**, 479 (1965)]; *Prog. Theor. Phys.* **44**, 291 (1970).

[2] N. Cabibbo, G. Parisi, *Phys. Lett.* **B59**, 67 (1975); J.C. Collins, M.J. Perry, *Phys. Rev. Lett.* **34**, 1353 (1975).

[3] E.V. Shuryak, *Phys. Rep.* **61**, 71 (1980).

[4] M. Gazdzicki, M.I. Gorenstein, *Acta Phys. Pol. B* **30**, 2705 (1999) [arXiv:hep-ph/9803462].

[5] C. Alt *et al.* [NA49 Collaboration], *Phys. Rev.* **C77**, 024903 (2008) [arXiv:0710.0118 [nucl-ex]]. A report for non-experts may be found in: M. Gazdzicki, R. Stock, P. Seyboth, *CERN Courier*, Vol. **43**, No. 3, 17 (2003).

[6] J. Pochodzalla *et al.*, *Phys. Rev. Lett.* **75**, 1040 (1995).

[7] http://cern.web.cern.ch/CERN/Announcements/2000/NewStateMatter/

[8] J. Rafelski, B. Muller, *Phys. Rev. Lett.* **48**, 1066 (1982) [Erratum-ibid. **56**, 2334 (1986)]; P. Koch, B. Müller, J. Rafelski, *Phys. Rep.* **142**, 167 (1986).

[9] T. Matsui, H. Satz, *Phys. Lett.* **B178**, 416 (1986).

[10] M. Gazdzicki, D. Roehrich, *Z. Phys.* **C65**, 215 (1995).

[11] M. Gazdzicki, D. Roehrich, *Z. Phys.* **C71**, 55 (1996) [arXiv:hep-ex/9607004].

[12] P. Seyboth [NA49 Collaboration], Addedndum-1 to the NA49 Proposal, CERN-SPSC-97-26; M. Gazdzicki, arXiv:nucl-th/9701050.

[13] M. Gazdzicki, *J. Phys. G* **30**, S161 (2004) [arXiv:hep-ph/0305176].

[14] L. Van Hove, *Phys. Lett.* **B118**, 138 (1982).

[15] C.M. Hung, E.V. Shuryak, *Phys. Rev. Lett.* **75**, 4003 (1995) [arXiv:hep-ph/9412360]; C.M. Hung, E.V. Shuryak, *Phys. Rev.* **C57**, 1891 (1998) [arXiv:hep-ph/9709264].

[16] M.I. Gorenstein, M. Gazdzicki, K.A. Bugaev, *Phys. Lett.* **B567**, 175 (2003) [arXiv:hep-ph/0303041].

[17] M. Gazdzicki *et al.* [NA61/SHINE Collaboration], *PoS* **CPOD2006**, 016 (2006).

[18] N. Antoniou *et al.* [NA61/SHINE Collaboration], CERN-SPSC-2006-034.

[19] G.S.F. Stephans, *J. Phys. G* **32**, S447 (2006) [arXiv:nucl-ex/0607030].

[20] P. Senger *et al.*, *PoS* **CPOD2006**, 018 (2006).

[21] A.N. Sissakian, A.S. Sorin, V.D. Toneev, arXiv:nucl-th/0608032.

[22] M. Bleicher, arXiv:hep-ph/0509314; H. Petersen, M. Bleicher, *PoS* **CPOD2006**, 025 (2006) [arXiv:nucl-th/0611001].

[23] M. Gazdzicki, M.I. Gorenstein, S. Mrowczynski, *Phys. Lett.* **B585**, 115 (2004) [arXiv:hep-ph/0304052].

[24] M.I. Gorenstein, M. Gazdzicki, O.S. Zozulya, *Phys. Lett.* **B585**, 237 (2004) [arXiv:hep-ph/0309142].

[25] J. Baechler *et al.* [NA35 Collaboration], *Phys. Rev. Lett.* **72**, 1419 (1994).

[26] H. Leutwyler, *Phys. Lett.* **B378**, 313 (1996) [arXiv:hep-ph/9602366].

[27] J. Cleymans, R.V. Gavai, E. Suhonen, *Phys. Rep.* **130**, 217 (1986).

[28] M. Gazdzicki, *Z. Phys.* **C66**, 659 (1995); M. Gazdzicki, *J. Phys. G* **23**, 1881 (1997) [arXiv:nucl-th/9706036].

[29] M. Gazdzicki, M.I. Gorenstein, S. Mrowczynski, *Eur. Phys. J.* **C5**, 129 (1998) [arXiv:nucl-th/9701013].

[30] J.I. Kapusta, A. Mekjian, *Phys. Rev.* **D33**, 1304 (1986).

[31] T. Matsui, B. Svetitsky, L.D. McLerran, *Phys. Rev.* **D34**, 2047 (1986); T. Matsui, B. Svetitsky, L.D. McLerran, *Phys. Rev.* **D34**, 783 (1986) [Erratum-ibid. **D37**, 844 (1988)].

[32] J. Rafelski, M. Danos, *Phys. Lett.* **B97**, 279 (1980).

[33] H. Bialkowska, M. Gazdzicki, W. Retyk, E. Skrzypczak, *Z. Phys.* **C55**, 491 (1992).

[34] D. Teaney, J. Lauret, E.V. Shuryak, *Phys. Rev. Lett.* **86**, 4783 (2001) [arXiv:nucl-th/0011058].

[35] M.I. Gorenstein, K.A. Bugaev, M. Gazdzicki, *Phys. Rev. Lett.* **88**, 132301 (2002) [arXiv:hep-ph/0112197]; K.A. Bugaev, M. Gazdzicki, M.I. Gorenstein, *Phys. Lett.* **B544**, 127 (2002) [arXiv:hep-ph/0206109]; K.A. Bugaev, M. Gazdzicki, M.I. Gorenstein, *Phys. Rev.* **C68**, 017901 (2003) [arXiv:hep-ph/0211337].

[36] L.D. Landau, *Izv. Akad. Nauk Ser. Fiz.* **17**, 51 (1953).

[37] S.Z. Belenkij, L.D. Landau, *Nuovo Cim. Suppl.* **3S10**, 15 (1956) [*Usp. Fiz. Nauk* **56**, 309 (1955)].

[38] C. Alt *et al.* [NA49 Collaboration], *Phys. Rev.* **C79**, 044910 (2009) [arXiv:0808.1237 [nucl-ex]].

[39] E.V. Shuryak, *Yad. Fiz.* **16**, 395 (1972).

[40] P. Carruthers, In *New York 1973, Annals of The New York Academy of Sciences*, Vol.229, New York 1974, 91–123 and Cornell Univ Ithaca — CLNS-219 (73, REC.APR), p. 51.

[41] C. Blume, *J. Phys. G* **31**, S57 (2005).

[42] J.L. Klay *et al.* [E-0895 Collaboration], *Phys. Rev.* **C68**, 054905 (2003) [arXiv:nucl-ex/0306033].

[43] I.G. Bearden *et al.* [BRAHMS Collaboration], *Phys. Rev. Lett.* **94**, 162301 (2005) [arXiv:nucl-ex/0403050].

[44] C.M. Hung, E.V. Shuryak, *Phys. Rev. Lett.* **75**, 4003 (1995) [arXiv:hep-ph/9412360].

[45] D.H. Rischke *et al.*, *Heavy Ion Phys.* **1**, 309 (1995) [arXiv:nucl-th/9505014].

[46] J. Brachmann, A. Dumitru, H. Stoecker, W. Greiner, *Eur. Phys. J.* **A8**, 549 (2000) [arXiv:nucl-th/9912014].

[47] C. Alt *et al.* [NA49 Collaboration], *Phys. Rev.* **C78**, 034914 (2008) [arXiv:0712.3216 [nucl-ex]].

[48] C. Alt *et al.* [NA49 Collaboration], *Phys. Rev.* **C79**, 044910 (2009) [arXiv:0808.1237 [nucl-ex]].

[49] J. Letessier, J. Rafelski, *Eur. Phys. J.* **A35**, 221 (2008) [arXiv:nucl-th/0504028].

[50] J.K. Nayak *et al.*, *Acta Phys. Slov.* **56**, 27 (2006).

[51] S.V. Akkelin, Yu.M. Sinyukov, *Phys. Rev.* **C73**, 034908 (2006) [arXiv:nucl-th/0505045].

[52] B. Abelev *et al.* [STAR Collaboration], *Phys. Rev. Lett.* **103**, 251601 (2009).

[53] D. Kharzeev, R.D. Pisarski, M.H.G. Tytgat, *Phys. Rev. Lett.* **81**, 512 (1998) [arXiv:hep-ph/9804221].

[54] R. Hagedorn, CERN report CERN-TH-7190-94 and Proceedings of NATO Advanced Study Workshop on Hot Hadronic Matter: Theory and Experiment, Divonne-les-Bains, Switzerland, June 27–July 1, 1994, ed. J. Letessier, H. Gutbrod, J. Rafelski, [Hot Hadronic Matter, v. **346**, 13 (1995)]; J. Cleymans, H. Satz, *Z. Phys.* **C57**, 135 (1993); J. Sollfrank, M. Gaździcki, U. Heinz, J. Rafelski, *Z. Phys.* **C61**, 659 (1994); P. Braun-Munzinger, J. Stachel, J. Wessels, N. Xu, *Phys. Lett.* **B365**, 1 (1996); G.D. Yen, M.I. Gorenstein, W. Greiner, S.N. Yang, *Phys. Rev.* **C56**, 2210 (1997); F. Becattini, U.W. Heinz, *Z. Phys.* **C76**, 269 (1997); G.D. Yen, M.I. Gorenstein, *Phys. Rev.* **C59**, 2788 (1999).

[55] J. Cleymans, K. Redlich, *Phys. Rev.* **C60**, 054908 (1999) [arXiv:nucl-th/9903063]; P. Braun-Munzinger, J. Cleymans, H. Oeschler, K. Redlich, *Nucl. Phys.* **A697**, 902 (2002) [arXiv:hep-ph/0106066].

[56] F. Becattini, M. Gazdzicki, J. Sollfrank, *Eur. Phys. J.* **C5**, 143 (1998) [arXiv:hep-ph/9710529].

[57] F. Becattini *et al.*, *Phys. Rev.* **C69**, 024905 (2004).

[58] F. Becattini, J. Manninen, M. Gazdzicki, *Phys. Rev.* **C73**, 044905 (2006).

[59] A. Andronic, P. Braun-Munzinger, J. Stachel, *Nucl. Phys.* **A834**, 237C (2010) [arXiv:0911.4931 [nucl-th]].

[60] H. Sorge, H. Stocker, W. Greiner, *Nucl. Phys.* **A498**, 567 (1989).

[61] S.A. Bass *et al.*, *Prog. Part. Nucl. Phys.* **41**, 225 (1998) [arXiv:nucl-th/9803035].

[62] W. Cassing, E.L. Bratkovskaya, S. Juchem, *Nucl. Phys.* **A674**, 249 (2000) [arXiv:nucl-th/0001024].

[63] F. Wang *et al.*, *Phys. Rev.* **C61**, 064904 (2000) [arXiv:nucl-th/9909001].

[64] H. Weber, E.L. Bratkovskaya, H. Stoecker, *Phys. Lett.* **B545**, 285 (2002).

[65] E.L. Bratkovskaya *et al.*, *Phys. Rev.* **C69**, 054907 (2004).

[66] B. Tomasik, E.E. Kolomeitsev, *Eur. Phys. J.* **C49**, 115 (2007).

[67] S. Kniege *et al.* [NA49 Collaboration], *J. Phys. G* **30**, S1073 (2004).

[68] C. Alt *et al.* [NA49 Collaboration], *Phys. Rev.* **C77**, 064908 (2008) [arXiv:0709.4507 [nucl-ex]].

[69] Yu.B. Ivanov, V.N. Russkikh, *Eur. Phys. J.* **A37**, 139 (2008) [arXiv:nucl-th/0607070].

[70] U.W. Heinz, *J. Phys. Conf. Ser.* **50**, 230 (2006) [arXiv:nucl-th/0504011].

[71] M. Gazdzicki *et al.*, *Braz. J. Phys.* **34**, 322 (2004) [arXiv:hep-ph/0309192].

[72] V.V. Begun, M. Gazdzicki, M.I. Gorenstein, *Phys. Rev.* **C78**, 024904 (2008) [arXiv:0804.0075 [hep-ph]].

[73] B.I. Abelev *et al.* [STAR Collaboration], *Phys. Rev.* **C81**, 024911 (2010) [arXiv:0909.4131 [nucl-ex]].

[74] T. Alber *et al.* [NA35 Collaboration], *Z. Phys.* **C64**, 195 (1994).

[75] M. Mitrovski [NA49 Collaboration], Ph.D. Thesis, University of Frankfurt, 2007.

[76] C. Baglin *et al.* [NA38 Collaboration], *Phys. Lett.* **B220**, 471 (1989); M.C. Abreu *et al.* [NA50 Collaboration], *Phys. Lett.* **B477**, 28 (2000); R. Arnaldi *et al.* [NA60 Collaboration], *Phys. Rev. Lett.* **99**, 132302 (2007).

[77] M. Gazdzicki, M.I. Gorenstein, *Phys. Rev. Lett.* **83**, 4009 (1999) [arXiv:hep-ph/9905515].

[78] P. Braun-Munzinger, J. Stachel, *Phys. Lett.* **B490**, 196 (2000) [arXiv:nucl-th/0007059].

[79] M.I. Gorenstein, A.P. Kostyuk, H. Stoecker, W. Greiner, *Phys. Lett.* **B524**, 265 (2002) [arXiv:hep-ph/0104071].

[80] M.G. Alford, K. Rajagopal, F. Wilczek, *Phys. Lett.* **B422**, 247 (1998) [arXiv:hep-ph/9711395]; L. McLerran, R.D. Pisarski, *Nucl. Phys.* **A796**, 83 (2007) [arXiv:0706.2191 [hep-ph]].

[81] J.I. Kapusta, E.S. Bowman, *PoS* **CPOD2009**, 018 (2009) [arXiv:0908.0726 [nucl-th]].

[82] M.A. Stephanov, K. Rajagopal, E.V. Shuryak, *Phys. Rev. Lett.* **81**, 4816 (1998) [arXiv:hep-ph/9806219].